Inclusion of the long-range proton-proton Coulomb force in the three-nucleon scattering Faddeev calculations

H. Witała, J. Golak, and R. Skibiński
M. Smoluchowski Institute of Physics, Jagiellonian University, PL-30348 Kraków, Poland

(Received 5 October 2023; revised 5 July 2024; accepted 14 August 2024; published 30 August 2024)

We propose a simplified approach to incorporate the long-range proton-proton (*pp*) Coulomb force in three-nucleon (3N) scattering calculations, based on the exact formulation presented by Witała, Skibiński, Golak, and Glöckle [Eur. Phys. J. A **41**, 369 (2009) and Eur. Phys. J. A **41**, 385 (2009)]. It permits us to get elastic proton-deuteron (*pd*) scattering and breakup observables relatively simply by performing standard Faddeev calculations as known for the neutron-deuteron (*nd*) system. The basic ingredient in that approach is a three-dimensional screened *pp* Coulomb t-matrix obtained by numerical solution of the three-dimensional Lippmann-Schwinger (LS) equation. Based on this t-matrix, pure Coulomb transition terms contributing to elastic scattering and breakup are calculated without any need for partial-wave decomposition. For elastic scattering such a term removes the Rutherford amplitude for point deuteron proton-deuteron (*pd*) scattering. For breakup it provides contributions which are important in some regions of the breakup phase space. We demonstrate numerically that the *pd* elastic observables can be determined directly from the resulting 3N amplitudes without any renormalization, simply by increasing the screening radius in order to reach the existing screening limit. However, for *pd* breakup the renormalization of the contributing on-shell amplitudes is required. We apply our approach in a wide energy range of the incoming proton for *pd* elastic scattering as well as for the *pd* breakup reaction.

DOI: 10.1103/PhysRevC.110.024005

I. INTRODUCTION

For a long time the problem of how to include the Coulomb force in the analysis of nuclear reactions with more than two nucleons has attracted wide attention. The main difficulty is the long-range nature of the Coulomb force which prevents the application of the standard techniques developed for short-range interactions. One possible way to include the Coulomb force is to use a screened Coulomb interaction and to reach the pure Coulomb limit through application of a renormalization procedure [1–4].

The high quality of the available *pd* data for elastic scattering and for the deuteron breakup reaction below the pion production threshold requires a theoretical analysis with the *pp* Coulomb force included in the calculations performed with modern nuclear forces. For this three-nucleon (3N) system using the Faddeev scheme high-precision numerical predictions for different observables in both processes have been obtained [5], but only under the restriction to short-ranged nuclear interactions.

First results for elastic *pd* scattering with modern nuclear forces and the Coulomb force included were provided in a variational hyperspherical harmonic approach [6]. The inclusion of the Coulomb force became possible in addition to elastic *pd* scattering also for the *pd* breakup reaction [7]. In [6] the exact Coulomb force in coordinate representation was used directly. In contrast to [7] a screened *pp* Coulomb force was applied in momentum space and in a partial-wave basis. In order to get the final predictions which can be compared to the data, the limit to the unscreened situation was taken numerically, applying a renormalization to the resulting 3N on-shell amplitudes [7–9]. This allowed the authors for the first time to analyze high-precision *pd* breakup data together with higher energy *pd* elastic scattering ones, and provided a significant improvement of data description in the cases where the Coulomb force plays an important role, see e.g. [10].

In spite of the breakthrough in the *pd* breakup treatment achieved in [7–9] some important questions concerning data description remained unanswered. One is the inability to understand the *pp* quasi-free-scattering (QFS) and pd space-star (SST) cross sections (see Introduction in [11]). It motivated us to reconsider the inclusion of the Coulomb force in momentum space Faddeev calculations. The main concern in such type of calculations is the application of a partial-wave decomposition to the long-ranged Coulomb force. Even when screening is applied, it seems reasonable to treat from the beginning the screened *pp* Coulomb t-matrix without partial-wave decomposition, because the required limit of vanishing screening leads necessarily to a drastic increase of the number of partial-wave states involved, what in consequence makes the number of 3N partial waves required for convergence extremely large. That fact prompted us to develop in [11] a novel approach to incorporate the *pp* Coulomb force in the momentum space 3N Faddeev calculations. It is based on a standard formulation for short-range forces and relies on the screening of the long-range Coulomb interaction. In order to avoid all uncertainties connected with the application of the partial-wave expansion, inevitable when

working with long-range forces, we used directly the three-dimensional *pp* screened Coulomb t-matrix. We demonstrated the feasibility of that approach in the case of elastic *pd* scattering using a simple dynamical model for the nuclear part of the interaction. It turned out that the screening limit exists without the need of renormalization not only for *pd* elastic scattering observables but for the elastic *pd* amplitude itself. In [11] we demonstrated that the physical *pd* elastic scattering amplitude can be obtained from the off-shell solutions of the Faddeev equation and has a well defined screening limit.

In [12] we extended that approach to *pd* breakup. Again we applied directly the three-dimensional screened *pp* Coulomb t-matrix without relying on a partial-wave decomposition. In contrast to elastic scattering, where the amplitude itself does not require renormalization, in the case of *pd* breakup the on-shell solutions of the Faddeev equation are required, which necessitates renormalization in the screening limit.

In our approach it is possible to obtain the elastic scattering amplitudes as well as observables without any renormalization, in contrast to the method of Refs. [7,8], where the elastic scattering amplitudes are obtained as a solution of Alt-Grassberger-Sandhas (AGS) equations and where renormalization is unavoidable. The reason is the interplay between the proton-proton Coulomb interaction and the deuteron bound-state pole in the AGS equations [13]. In contrast to that, in our approach we calculate the elastic scattering amplitudes using solutions of the 3N Faddeev equations, whose structure guarantees that solutions import properties of the two-nucleon t-matrices. The fact that elastic *pd* scattering requires only off-shell solutions of the Faddeev equations and that the off-shell two-nucleon t-matrices have well defined screening limits is the reason why in our method no renormalization is needed. It should be emphasized that both approaches are exact and should lead to the same results for observables in the *pd* elastic scattering and breakup reactions.

The main purpose of present investigation is to establish a relatively fast and simple calculational scheme for getting reliable estimation of the *pp* Coulomb force effects in *pd* reactions, which will be with respect to the required time and computer resources comparable to the standard *nd* Faddeev calculations. In our exact approach of Refs. [11,12] the need to calculate a number of complex terms, whose determination is very demanding with respect to the required computer time and resources, makes this approach difficult. In view of coming challenges, such as fine tuning of chiral forces by using high precision *pd* data, a simpler and faster method for calculation of *pd* reactions is required.

In Sec. II for the convenience of the reader we briefly present the main points of the formalism outlined in detail in [11,12] and introduce our simplified calculational scheme. The numerical results for *pd* elastic scattering are presented and discussed in Sec. III A and for breakup in Sec. III B. The summary and conclusions are given in Sec. IV.

II. SCREENED *pp* COULOMB FORCE IN FADDEEV EQUATIONS

In the following we describe our simplified treatment, which arises from the exact formulation of Refs. [11,12]. For the convenience of the reader we repeat the main steps of [11,12].

We regard the 3N *pd* system in the isospin basis where the two-body isospin t together with the isospin $\frac{1}{2}$ of the third particle is coupled to the total isospin T and the corresponding completeness relation is [the convention assumed is that the proton (neutron) has the isospin magnetic quantum number $-\frac{1}{2}$ ($\frac{1}{2}$)]:

$$\sum_{tT} |(t\,1/2)T\,-\,1/2\rangle\langle(t\,1/2)T\,-\,1/2| = I. \tag{1}$$

We use the Faddeev equation in the form when nucleons interact with pairwise forces only [5]:

$$T|\Phi\rangle = tP|\Phi\rangle + tPG_0T|\Phi\rangle, \tag{2}$$

where P is defined in terms of transposition operators, $P = P_{12}P_{23} + P_{13}P_{23}$, G_0 is the free 3N propagator, $|\Phi\rangle$ the initial state composed of a deuteron state and a momentum eigenstate of the proton. The t-matrix t is a solution of the two-body Lippmann-Schwinger (LS) equation,

$$t = V + VG_0t, \tag{3}$$

with the interaction V containing the neutron-proton (np) ($V^{t0}_{np} = \langle t0|V|t0\rangle$) and pp ($V^{1-1}_{pp} = \langle 1-1|V|1-1\rangle$) potentials [14]. The pp interaction decomposes into the strong part and the pure Coulomb part (assumed to be screened and parametrized by some parameter R),

$$V^{1-1}_{pp} = V^{\text{strong}}_{pp} + V^{cR}_{pp}. \tag{4}$$

Since the presence of the pp Coulomb force induces large charge independence breaking, which leads necessarily to coupling of $T = 1/2$ and $T = 3/2$ states [14], the complete treatment of the Coulomb force requires states with both total isospin values.

Knowing $T|\Phi\rangle$ the breakup as well as the elastic *pd* scattering amplitudes can be gained by quadratures in the standard manner [5]. We solve Faddeev equations in our momentum space partial wave basis $|pq\alpha\rangle$,

$$|pq\alpha\rangle \equiv \left|pq(ls)j\left(\lambda\tfrac{1}{2}\right)I(jI)J\left(t\tfrac{1}{2}\right)T\right\rangle, \tag{5}$$

distinguishing between the partial-wave states $|pq\alpha\rangle$ with total 2N angular momentum j below some value $j_{\max}$, $j \leqslant j_{\max}$, in which the nuclear, V_N, as well as the pp screened Coulomb interaction, V^R_c (in isospin $t = 1$ states only), act, and the states $|pq\beta\rangle$ with $j > j_{\max}$, for which only V^R_c acts in the pp subsystem. The states $|pq\alpha\rangle$ and $|pq\beta\rangle$ form a complete system of states:

$$\int p^2dp\,q^2dq\left(\sum_\alpha |pq\alpha\rangle\langle pq\alpha| + \sum_\beta |pq\beta\rangle\langle pq\beta|\right) = I. \tag{6}$$

Projecting Eq. (2) for $T|\Phi\rangle$ on the $|pq\alpha\rangle$ and $|pq\beta\rangle$ states one gets the following system of coupled integral equations (in the following we use a shorthand notation

$\sum_\alpha \int p^2 dp\, q^2 dq |pq\alpha\rangle\langle pq\alpha| \equiv \sum_\alpha \int |\alpha\rangle\langle\alpha|$):

$$\begin{aligned}\langle pq\alpha|T|\Phi\rangle &= \langle pq\alpha|t^R_{N+c}P|\Phi\rangle + \langle pq\alpha|t^R_{N+c}PG_0\sum_{\alpha'}\int|\alpha'\rangle\langle\alpha'|T|\Phi\rangle \\ &\quad + \langle pq\alpha|t^R_{N+c}PG_0\sum_{\beta'}\int|\beta'\rangle\langle\beta'|T|\Phi\rangle, \qquad (7)\\ \langle pq\beta|T|\Phi\rangle &= \langle pq\beta|t^R_{c}P|\Phi\rangle + \langle pq\beta|t^R_{c}PG_0\sum_{\alpha'}\int|\alpha'\rangle\langle\alpha'|T|\Phi\rangle \\ &\quad + \langle pq\beta|t^R_{c}PG_0\sum_{\beta'}\int|\beta'\rangle\langle\beta'|T|\Phi\rangle, \qquad (8)\end{aligned}$$

where t^R_{N+c} and t^R_c are t-matrices generated by the interactions $V_N + V^R_c$ and V^R_c, respectively. For states $|\alpha\rangle$ with two-nucleon subsystem isospin $t = 1$ the corresponding t-matrix element $\langle p\alpha|t^R_{N+c}(E - \frac{3}{4m}q^2)|p'\alpha'\rangle$ is a linear combination of the pp, t^R_{pp+c}, and the neutron-proton (np), t_{np}, $t = 1$ t-matrices, which are generated by the interactions $V^{\rm strong}_{pp} + V^R_c$ and $V^{\rm strong}_{np}$, respectively. The coefficients of that combination depend on the total isospin T and T' of states $|\alpha\rangle$ and $|\alpha'\rangle$ [11,14]:

$$\begin{aligned}\left\langle t=1\ T=\tfrac12\middle|t^R_{N+c}\middle|t'=1\ T'=\tfrac12\right\rangle &= \tfrac13 t_{np} + \tfrac23 t^R_{pp+c}\\ \left\langle t=1\ T=\tfrac32\middle|t^R_{N+c}\middle|t'=1\ T'=\tfrac32\right\rangle &= \tfrac23 t_{np} + \tfrac13 t^R_{pp+c}\\ \left\langle t=1\ T=\tfrac12\middle|t^R_{N+c}\middle|t'=1\ T'=\tfrac32\right\rangle &= \tfrac{\sqrt2}{3}\left(t_{np} - t^R_{pp+c}\right)\\ \left\langle t=1\ T=\tfrac32\middle|t^R_{N+c}\middle|t'=1\ T'=\tfrac12\right\rangle &= \tfrac{\sqrt2}{3}\left(t_{np} - t^R_{pp+c}\right). \qquad (9)\end{aligned}$$

For isospin $t = 0$, where $T = T' = \frac12$,

$$\left\langle t=0\ T=\tfrac12\middle|t^R_{N+c}\middle|t'=0\ T'=\tfrac12\right\rangle = t_{np}. \qquad (10)$$

In the case of t^R_c only the screened pp Coulomb force V^R_c acts.

The third term on the right-hand side of (8) is proportional to $\langle pq\beta|t^R_c PG_0|p'q'\beta'\rangle\langle p'q'\beta'|t^R_c$. A direct calculation shows that it vanishes, independently of the value of the total isospin T.

Inserting $\langle pq\beta|T|\Phi\rangle$ from (8) into (7) and using (6) one gets

$$\begin{aligned}\langle pq\alpha|T|\Phi\rangle &= \langle pq\alpha|t^R_{N+c}P|\Phi\rangle + \langle pq\alpha|t^R_{N+c}PG_0t^R_cP|\Phi\rangle\\ &\quad - \langle pq\alpha|t^R_{N+c}PG_0\sum_{\alpha'}\int|\alpha'\rangle\langle\alpha'|t^R_cP|\Phi\rangle\\ &\quad + \langle pq\alpha|t^R_{N+c}PG_0\sum_{\alpha'}\int|\alpha'\rangle\langle\alpha'|T|\Phi\rangle\\ &\quad + \langle pq\alpha|t^R_{N+c}PG_0t^R_cPG_0\sum_{\alpha'}\int|\alpha'\rangle\langle\alpha'|T|\Phi\rangle\\ &\quad - \langle pq\alpha|t^R_{N+c}PG_0\sum_{\alpha'}\int|\alpha'\rangle\langle\alpha'|t^R_cPG_0\\ &\quad \times\sum_{\alpha''}\int|\alpha''\rangle\langle\alpha''|T|\Phi\rangle. \qquad (11)\end{aligned}$$

This is a coupled set of integral equations in the space of only the states $|\alpha\rangle$, which exactly incorporates the contributions of the pp Coulomb interaction from all partial-wave states up to infinity. It can be solved by iteration and Padé summation. However, the very time consuming and complicated calculation of contributing terms containing the three-dimensional screened Coulomb t-matrix (the second and fifth terms) prevents solution of that equation for the practically interesting case of sufficiently large partial-wave basis. It is our aim in the present investigation to simplify (11) without losing its physical content, so that the resulting equation will be manageable as for the nd system.

Actually a glimpse at Eq. (11) reveals a possibility to avoid completely a calculation of these complicated terms with a three-dimensional Coulomb t-matrix and to omit the second, third, as well as the fifth and sixth terms altogether. Namely, at a specific value of the screening radius R, a finite set of partial waves provides an exact reproduction of the three-dimensional Coulomb t-matrix t^R_c. Extending the set $|\alpha\rangle$ to such a set of states by adding a finite number of channels with higher angular momenta, in which only the pp Coulomb interaction is present, permits one to completely neglect the above mentioned four terms due to their mutual cancellation: the second term with the third, and the fifth term with the sixth. The set (11) is then reduced to the identical form as in the nd case

$$\begin{aligned}\langle pq\alpha|T|\Phi\rangle &= \langle pq\alpha|t^R_{N+c}P|\Phi\rangle + \langle pq\alpha|t^R_{N+c}PG_0\sum_{\alpha'}\int|\alpha'\rangle\langle\alpha'|T|\Phi\rangle. \qquad (12)\end{aligned}$$

With an increasing R value the above cancellation requires more and more partial waves, so generally for a finite set $|\alpha\rangle$ only a partial cancellation is expected, making (12) only an approximation to the exact formulation (11). In the following we will refer to (12) as "simplified approach (12)" [SA(12)].

Even in the case when channels $|\alpha\rangle$ are those in which nuclear and pp Coulomb forces act and only partial cancellation occurs, an additional argument prompts one to simplify the set (7)–(8). Namely, in Eqs. (7) and (8) the strength of the coupling between amplitudes $\langle pq\alpha|T|\Phi\rangle$ and $\langle pq\beta|T|\Phi\rangle$ is determined by matrix elements of the permutation operator $\langle pq\alpha|P|p'q'\beta\rangle$. Since channels $|\beta\rangle$ have values of the total two-body subsystem angular momentum j larger than those of the channels $|\alpha\rangle$, the matrix element of the permutation operator between these states is smaller than between $|\alpha\rangle$ states. One can thus argue that the third term in Eq. (7) and second in (8) are small compared to the leading terms. Neglecting them would lead again to the set (12).

For a restricted basis $|\alpha\rangle$ ($j \leqslant 3$) it is possible to compute the second term in (11) with the three-dimensional Coulomb t-matrix within a reasonable amount of computer time and resources. Therefore we would also like to look at these cancellations in a more direct way. By omitting only the second term in Eq. (8) one reduces (11) to a form containing the first pair of leading terms with the three-dimensional and its

partial-wave decomposed counterpart Coulomb t-matrix:

$$\langle pq\alpha|T|\Phi\rangle = \langle pq\alpha|t^R_{N+c}P|\Phi\rangle + \langle pq\alpha|t^R_{N+c}PG_0t^R_cP|\Phi\rangle - \langle pq\alpha|t^R_{N+c}PG_0\sum_{\alpha'}\int|\alpha'\rangle\langle\alpha'|t^R_cP|\Phi\rangle + \langle pq\alpha|t^R_{N+c}PG_0\sum_{\alpha'}\int|\alpha'\rangle\langle\alpha'|T|\Phi\rangle. \quad (13)$$

We will solve both Eqs. (12) and (13) and demonstrate how cancellation effects between the second and third terms in (11) affect the elastic scattering and breakup observables and how they justify the use of (12) and omission of the term with the three-dimensional t-matrix.

After solving 3N Faddeev equations the transition amplitude for elastic scattering is given by [5,15]

$$\langle\Phi'|U|\Phi\rangle = \langle\Phi'|PG_0^{-1} + PT|\Phi\rangle. \quad (14)$$

The first contribution is independent of the pp Coulomb force and can be calculated without partial-wave decomposition using the expression given in Appendix C of Ref. [11]. To calculate the second contribution in (14) one needs $\langle\vec{p}\vec{q}|T|\Phi\rangle$ composed of low (α) and high (β) partial-wave contributions for $T|\Phi\rangle$. Using the completeness relation (6) and Eq. (8) one gets

$$\langle\vec{p}\vec{q}\,|T|\Phi\rangle = \langle\vec{p}\vec{q}\,|\sum_{\alpha'}\int|\alpha'\rangle\langle\alpha'|T|\Phi\rangle - \langle\vec{p}\vec{q}\,|\sum_{\alpha'}\int|\alpha'\rangle\langle\alpha'|t^R_cP|\Phi\rangle + \langle\vec{p}\vec{q}\,|t^R_cP|\Phi\rangle - \langle\vec{p}\vec{q}\,|\sum_{\alpha'}\int|\alpha'\rangle\langle\alpha'|t^R_cPG_0\sum_{\alpha''}\int|\alpha''\rangle\langle\alpha''|T|\Phi\rangle + \langle\vec{p}\vec{q}\,|t^R_cPG_0\sum_{\alpha'}\int|\alpha'\rangle\langle\alpha'|T|\Phi\rangle. \quad (15)$$

It follows that in addition to the amplitudes $\langle pq\alpha|T|\Phi\rangle$ also the partial-wave projected amplitudes $\langle pq\alpha|t^R_cP|\Phi\rangle$ and $\langle pq\alpha|t^R_cPG_0|\alpha'\rangle\langle\alpha'|T|\Phi\rangle$ are required. The expressions for the contributions of these three terms to the transition amplitude for elastic scattering (and breakup) are given in Appendix B of Ref. [11]. The third and fifth terms in (15) must be calculated using directly the three-dimensional screened Coulomb t-matrices. Expressions for $\langle\vec{p}\vec{q}\,|t^R_cP|\Phi\rangle$ (breakup) and $\langle\Phi'|Pt^R_cP|\Phi\rangle$ (elastic scattering) are given in Appendix C of Ref. [11]. The term $\langle\Phi'|Pt^R_cP|\Phi\rangle$ for large values of the screening radius R is the contribution from the pp Coulomb force to the pd scattering, which corresponds to the Rutherford amplitude for point deuteron Coulomb pd scattering. The analogous term for breakup is $\langle\vec{p}\vec{q}\,|t^R_cP|\Phi\rangle$. The expression for the last matrix element $\langle\vec{p}\vec{q}|t^R_cPG_0|\alpha'\rangle\langle\alpha'|T|\Phi\rangle$ is given in Appendix D of Ref. [11]. It provides a correction to the pure Coulomb term in pd elastic scattering and breakup due to the strong interactions between nucleons. It is interesting to note that all terms containing a three-dimensional Coulomb t-matrix, both for elastic scattering and breakup, can be calculated using analytical expressions for the screening limit of that matrix.

Since we restrict ourselves to SA(12) and approach (13), it would seem validated to omit the fourth and fifth terms in Eq. (15), reducing it to

$$\langle\vec{p}\vec{q}\,|T|\Phi\rangle = \langle\vec{p}\vec{q}\,|\sum_{\alpha'}\int|\alpha'\rangle\langle\alpha'|T|\Phi\rangle - \langle\vec{p}\vec{q}\,|\sum_{\alpha'}\int|\alpha'\rangle\langle\alpha'|t^R_cP|\Phi\rangle + \langle\vec{p}\vec{q}\,|t^R_cP|\Phi\rangle. \quad (16)$$

Actually, there is no justification for rejecting these two pure Coulomb terms. On the contrary, it seems unavoidable that the pure Coulomb terms must receive contributions from strong interactions between nucleons as indicated by the second term in (8), the importance of which will probably depend on the energy. However, in the present investigation we stick first to approximation (16) for the transition amplitude, deferring the problem of importance of rejected terms for a later stage of the present study. In the following we will refer to (16) as "approximate transition amplitude (16)" [AA(16)] in contrast to "exact transition amplitude of Eq. (15)" [EA(15)].

The transition amplitude for breakup $\langle\Phi_0|U_0|\Phi\rangle$ is given in terms of $T|\Phi\rangle$ by [5,15]

$$\langle\Phi_0|U_0|\Phi\rangle = \langle\Phi_0|(1+P)T|\Phi\rangle, \quad (17)$$

where $|\Phi_0\rangle = |\vec{p}\vec{q}m_1m_2m_3\nu_1\nu_2\nu_3\rangle$ is the state of three free outgoing nucleons. The permutations acting in momentum, spin, and isospin spaces can be applied to the bra state $\langle\Phi_0| = \langle\vec{p}\vec{q}m_1m_2m_3\nu_1\nu_2\nu_3|$, changing the sequence of nucleons spin and isospin magnetic quantum numbers m_i and ν_i and leading to well known linear combinations of the Jacobi momenta $\vec{p},\vec{q}$. Thus evaluating (17) it is sufficient to regard the general amplitudes $\langle\vec{p}\vec{q}m_1m_2m_3\nu_1\nu_2\nu_3|T|\Phi\rangle \equiv \langle\vec{p}\vec{q}|T|\Phi\rangle$, which are given again by (16). Also for breakup, in addition to the amplitudes $\langle pq\alpha|T|\Phi\rangle$, the partial-wave projected amplitude $\langle pq\alpha|t^R_cP|\Phi\rangle$ is required. The expressions for the contributions of these two terms to the transition amplitude for the breakup reaction are given in Appendix B of Ref. [11]. The last term in (16) must be calculated using directly the three-dimensional screened Coulomb t-matrix. It corresponds to the Rutherford amplitude in elastic pd scattering. In Appendix C of Ref. [11] the expression for $\langle\vec{p}\vec{q}|t^R_cP|\Phi\rangle$ is provided.

The Faddeev equations (12) and (13) are well defined for any finite screening radius. The important challenge is to control the screening limit for the physical pd elastic scattering and breakup amplitudes (15). In the case of elastic scattering we provided in Ref. [11] arguments that the physical elastic pd scattering amplitude itself has a well defined screening limit and does not require renormalization. This was traced back to the fact that in order to get the elastic pd scattering amplitude it is sufficient to solve the Faddeev equations (12)–(13) for off-shell values of the Jacobi momenta,

$$\frac{p^2}{m} + \frac{3}{4m}q^2 \neq E. \quad (18)$$

The off-shell Faddeev amplitudes $\langle pq\alpha|T|\Phi\rangle$ of Eqs. (12)–(13) are determined by off-shell nucleon-nucleon t-matrix elements $t(p,p';E-\frac{3}{4m}q^2)$, which have a well defined

screening limit (see [11] as well as the discussion and examples in [12]). Also the off-shell three-dimensional pure Coulomb t-matrix is known analytically (see [16,17] and references therein):

$$\langle \vec{p}\,'|t_c^R\left(\frac{k^2}{m}\right)|\vec{p}\rangle \to \frac{e^2}{2\pi^2}\frac{1+I(x)}{(\vec{p}\,'-\vec{p})^2} \tag{19}$$

with

$$I(x)=\frac{1}{x}\left[{}_2F_1\left(1,i\eta;1+i\eta;\frac{x+1}{x-1}\right)-{}_2F_1\left(1,i\eta;1+i\eta;\frac{x-1}{x+1}\right)\right]$$

and

$$x^2=1+\frac{(p'^2-k^2)(p^2-k^2)}{k^2(\vec{p}\,'-\vec{p})^2},$$

where ${}_2F_1$ is a hypergeometric function [18]. Thus also the Coulomb term $\langle\Phi'|Pt_c^RP|\Phi\rangle$ has a well defined screening limit [19].

In contrast to pd elastic scattering the physical breakup amplitude (17) corresponds to the on-shell values of Jacobi momenta

$$\frac{p^2}{m}+\frac{3}{4m}q^2=E\equiv\frac{3}{4m}q_{\max}^2. \tag{20}$$

That means that the physical pd breakup amplitude (17) requires on-shell Faddeev amplitudes $\langle p_0q\alpha|T|\Phi\rangle$ together with the two, also on-shell, additional terms in (16), with $p_0=\sqrt{\frac{3}{4}(q_{\max}^2-q^2)}$. The on-shell Faddeev amplitudes can be obtained from the off-shell solutions $\langle pq\alpha|T|\Phi\rangle$ using (11), (12), or (13) (in the following referred to as ONSH2). These on-shell amplitudes together with additional, also on-shell, terms in (16) define the physical breakup amplitude (17). That in consequence requires half-shell t-matrix elements $t(p_0,p';\frac{p_0^2}{m})$ which are of three types: the partial-wave projected pure screened Coulomb t_c^R generated by V_c^R, the partial-wave projected t_{N+c}^R generated by $V_{\rm strong}+V_c^R$, and the three-dimensional screened Coulomb t-matrix elements.

It is well known [1,20,21] that in the screening limit $R\to\infty$ such half-shell t-matrices acquire an infinitely oscillating phase factor $e^{i\Phi_R(p)}$, where $\Phi_R(p)$ depends on the type of the screening. For the exponential screening

$$V_c^R(r)=\frac{\alpha}{r}e^{-(\frac{r}{R})^n}, \tag{21}$$

its form depends on two parameters, the screening radius R and the power n. At a given value n the pure Coulomb potential results for $R\to\infty$. As has been shown in [22] based on [23,24], the related phase $\Phi_n^R(p)$ is given as

$$\Phi_n^R(p)=-\eta\left[\ln(2pR)-\frac{\gamma}{n}\right]+\eta\sum_{k=1}^{\infty}\frac{(-1)^k}{knk!(2pR)^{kn}}, \tag{22}$$

where $\gamma=0.5772\ldots$ is the Euler number and $\eta=\frac{m_p\alpha}{2p}$ is the so-called Sommerfeld parameter.

That oscillatory phase factor appearing in the half-shell proton-proton t-matrices requires a careful treatment to get the screening limit for the $\langle p_0q\alpha|T|\Phi\rangle$ amplitudes. Namely for the states $|\alpha\rangle$ with the two-nucleon subsystem isospin $t=1$ the corresponding t-matrix element $\langle p_0\alpha|t_{N+c}^R(\frac{p_0^2}{m})|p'\alpha'\rangle$ is a linear combination of the pp and neutron-proton (np) $t=1$ t-matrices, with coefficients which depend on the total isospins T and T' of the states $|\alpha\rangle$ and $|\alpha'\rangle$ [see discussion after (8)]. It follows that to achieve the screening limit one needs to renormalize breakup amplitudes by removing from them the oscillatory phase factor induced by the half-shell pp t-matrix t_{pp+c}^R. The term in that linear combination coming with the np t-matrix t_{np} is not influenced by the pp Coulomb force. In [12] we erroneously suggested a renormalization in that combination before performing the action of the operators in (12) and (13). This is, however, incorrect since amplitudes obtained in this way do not fulfill the Faddeev equations and would lead to false results for breakup observables. The only proper place to perform renormalization is during calculation of the breakup transition amplitude.

The breakup transition amplitude is built up from three contributions due to the action of the $(1+P)$ operator in Eq. (17). For a given specification of outgoing nucleons imposed by experimental conditions, only one of these contributions corresponds to the case that the neutron is a spectator nucleon 1 and two protons form the interacting 2-3 pair (pp partition). When calculating breakup transition amplitude the summation over $t=1$ $|\alpha\rangle$ states with the total 3N isospin $T=\frac{1}{2}$ or $T=\frac{3}{2}$ provides that in that particular partition only the component of the breakup transition amplitude driven by the pp half-shell t-matrix will be left. In contrast, the two other partitions with the proton as a spectator nucleon 1 will contain only the component of the breakup transition amplitude driven by np half-shell t-matrix (np partitions).

To be more specific let us consider the contribution to the breakup transition amplitude from particular isospin $t=1$ channels α, which differ only in their total isospin value $T=\frac{1}{2}$ or $\frac{3}{2}$, in a partition defined by a spectator nucleon 1 with isospin projection ν_1 and nucleons 2 and 3 with isospin projections ν_2 and ν_3, respectively. In the following we keep only isospin quantum numbers. This contribution is proportional to

$$\sum_{T,T'}C(T)\,\langle\alpha_T|t_{N+c}^R|\alpha_{T'}\rangle\langle\alpha_{T'}|A|\Phi\rangle, \tag{23}$$

with $A|\Phi\rangle=(P+PG_0T)|\Phi\rangle$ in case of Eq. (12), and

$$C(T)\equiv\left\langle\tfrac{1}{2}\nu_2\tfrac{1}{2}\nu_3\middle|t=1\nu_2+\nu_3\right\rangle\left\langle t=1\nu_2+\nu_3\tfrac{1}{2}\nu_1\middle|T\,\nu_2+\nu_3+\nu_1\right\rangle.$$

That gives the contribution to the pp partition ($\nu_2=\nu_3=-\frac{1}{2}$, $\nu_1=+\frac{1}{2}$) to be proportional to t_{pp+c}^R:

$$t_{pp+c}^R\left[-\sqrt{\tfrac{2}{3}}\langle T'=\tfrac{1}{2}|A|\Phi\rangle+\tfrac{1}{\sqrt{3}}\langle T'=\tfrac{3}{2}|A|\Phi\rangle\right];$$

and the contribution to the np partition ($\nu_2=-\frac{1}{2}$, $\nu_3=+\frac{1}{2}$ or $\nu_2=+\frac{1}{2}$, $\nu_3=-\frac{1}{2}$, $\nu_1=-\frac{1}{2}$) to be proportional to t_{np}:

$$t_{np}\left[\tfrac{\sqrt{2}}{2\sqrt{3}}\langle T'=\tfrac{1}{2}|A|\Phi\rangle+\tfrac{1}{\sqrt{3}}\langle T'=\tfrac{3}{2}|A|\Phi\rangle\right].$$

That means that renormalization has to be done on the level of contributing breakup amplitudes by renormalizing the amplitude $\langle p_0 q\alpha|T|\Phi\rangle$ for the pp partition with the neutron as a spectator nucleon 1. The same concern applies to the renormalization of contributions from $\langle p_0 q\alpha|t_c^R P|\Phi\rangle$ and from the three-dimensional pp t-matrix $\langle \vec{p}_0\vec{q}|t_c^R P|\Phi\rangle$, whose terms, however, contribute only in a pp partition with the neutron as a spectator nucleon 1. Since the half-shell pure Coulomb t-matrix is analytically given by [25]

$$\langle \vec{p}\,'|t_c^R\left(\frac{k^2}{m}\right)|\vec{k}\rangle \to C_0 e^{i\sigma_0}\frac{k\eta}{\pi^2 q^2}\left(\frac{p'^2-k^2}{q^2}\right)^{i\eta} \tag{24}$$

with $\vec{q}=\vec{p}\,'-\vec{k}$, the pure Coulomb phase shift $\sigma_0=\Gamma(1+i\eta)$, and Coulomb penetrability $C_0^2=\frac{2\pi\eta}{e^{2\pi\eta}-1}$, also the renormalized term $\langle \vec{p}_0\vec{q}|t_c^R P|\Phi\rangle$ has a well defined screening limit [19].

Another possibility to get on-shell breakup amplitudes is offered by interpolations of the off-shell amplitudes to on-shell values of Jacobi momenta (referred to in the following as ONSH1). In contrast to the half shell, the off-shell t-matrix elements do not acquire such an oscillating phase and their screening limit is well defined. Thus also off-shell $\langle p'q'\alpha'|T|\Phi\rangle$ as well as off-shell $\langle p'q'\alpha'|t_c^R P|\Phi\rangle$ and a three-dimensional Coulomb t-matrix do not acquire such an oscillating phase and their screening limits are well defined. However, their half-shell counterparts obtained by interpolation from off-shell to on-shell values of Jacobi momenta will gain the oscillating phase in their "pp" components. These interpolated on-shell amplitudes must be thus also renormalized.

The above two ways to get on-shell breakup amplitudes should provide the same results for breakup observables. It offers an additional verification of numerics.

III. NUMERICAL RESULTS

A. Elastic scattering

We applied the above approaches using a dynamical model in which three nucleons interact with the AV18 nucleon-nucleon potential [26] restricted to act only in partial waves with $j\leqslant 3$. The only reason why we restricted ourselves to this rather small value of $j_{\max}=3$ is that we would like to compare results of our simplified approach SA(12) with that of Eq. (13). This requires computation of the second component in the leading term of (13) with a three-dimensional Coulomb t-matrix. With $j_{\max}=3$ the needed computer time and resources are definitely affordable. The pp Coulomb force was screened exponentially,

$$V_{pp}^{cR}(r)=\frac{e^2}{r}e^{-(\frac{r}{R})^n}, \tag{25}$$

with the screening radius R and $n=4$.

To investigate the screening limit $R\to\infty$ we generated a set of partial-wave decomposed t-matrices, t_c^R, based on the screened pp Coulomb force alone, or combined with the pp nuclear interaction, t_{N+c}^R, taking $R=5$, 10, 20, 30, and 40 fm. With that dynamical input we solved the simplified Faddeev equation SA(12) for the total angular momenta of the p-p-n system up to $J\leqslant\frac{31}{2}$ and both parities. With the same screening radii we generated the three-dimensional pure Coulomb t-matrices t_c^R by solving the three-dimensional LS equation. For $R=40$ fm we solved also Eq. (13) calculating additional two leading terms containing three-dimensional Coulomb t-matrix as well as its partial-wave projected counterpart.

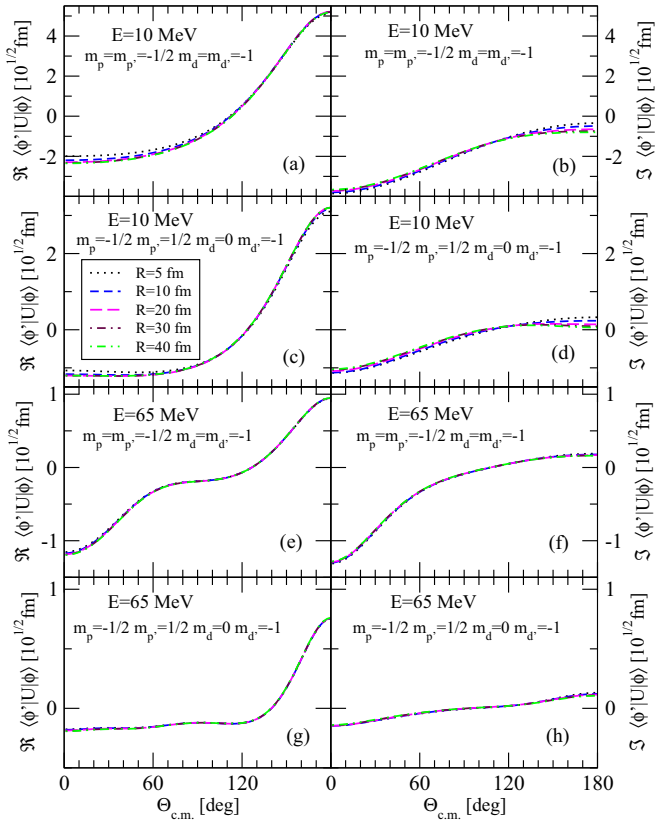

FIG. 1. Real (left side) and imaginary (right side) parts of non-renormalized pd elastic scattering amplitude $U=PT+PG_0^{-1}-Pt_c^R P-Pt_c^R PG_0 T$ based on solutions of SA(12), at $E_p=10$ MeV (a)–(d) and 65 MeV (e)–(h), shown as functions of the center-of-mass (c.m.) scattering angle. The initial and final proton and deuteron spin projection quantum numbers are indicated in the figure. Results for the AV18 NN potential obtained with the screening radii $R=5$ fm (black dotted lines), $R=10$ fm (blue short-dashed lines), $R=20$ fm (magenta long dashed lines), $R=30$ fm (maroon dashed-dotted lines), and $R=40$ fm (green double-dotted-dashed lines) are shown.

To start with we would like to show that indeed elastic scattering amplitudes in our approach do not require renormalization. This is exemplified for two energies, $E=10$ MeV and $E=65$ MeV, in Fig. 1, where real and imaginary parts of elastic scattering amplitudes are shown as a function of c.m. scattering angle for five values of the screening radius, $R=5$, 10, 20, 30, and 40 fm. Fast convergence in R for real and imaginary parts proves that renormalization is indeed superfluous in our approach.

In Fig. 2 we show the convergence in the screening radius R of the pd elastic scattering cross section. The pd predictions of the SA(12) approach, using approximate elastic scattering transition amplitude AA(16) with the Coulomb term, $\langle\Phi'|Pt_c^R P|\Phi\rangle$, calculated taking the corresponding screening

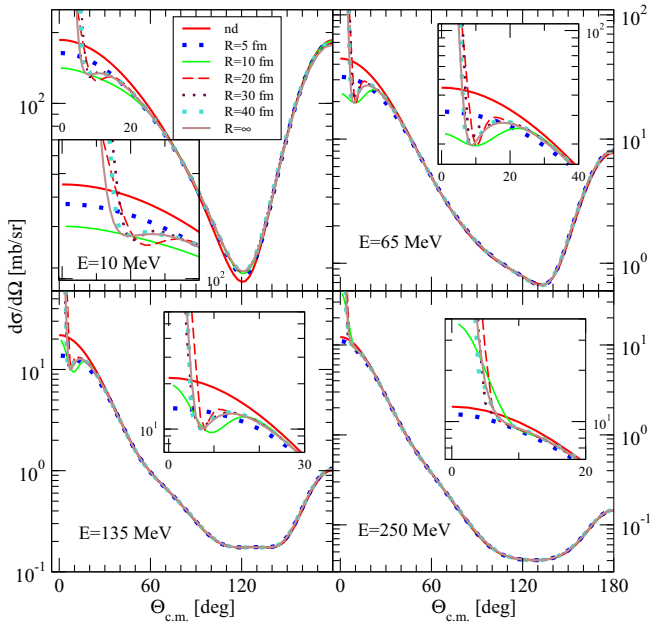

FIG. 2. The convergence in the cutoff radius R of the *pd* elastic scattering cross section $\frac{d\sigma}{d\Omega}$ shown as a function of the c.m. angle $\Theta_{\rm c.m.}$ at the incoming laboratory proton energies $E = 10$, 65, 135, and 250 MeV. These cross sections were calculated using approach SA(12) and taking elastic scattering transition amplitude AA(16) with the screened Coulomb force and the AV18 nucleon-nucleon potential [26] restricted to the $j \leqslant 3$ partial waves. The screening radii are $(n = 4)$ $R = 5$ fm (blue dotted line), $R = 10$ fm (green solid line), $R = 20$ fm (red long-dashed line), $R = 30$ fm (maroon dotted line), $R = 40$ fm (turquoise dotted line). The brown solid line corresponds to the $R = 40$ fm result with the three-dimensional Coulomb t-matrix t_c calculated according to Eq. (19). The red solid line is the nd elastic scattering cross section and the insets show the region of small angles.

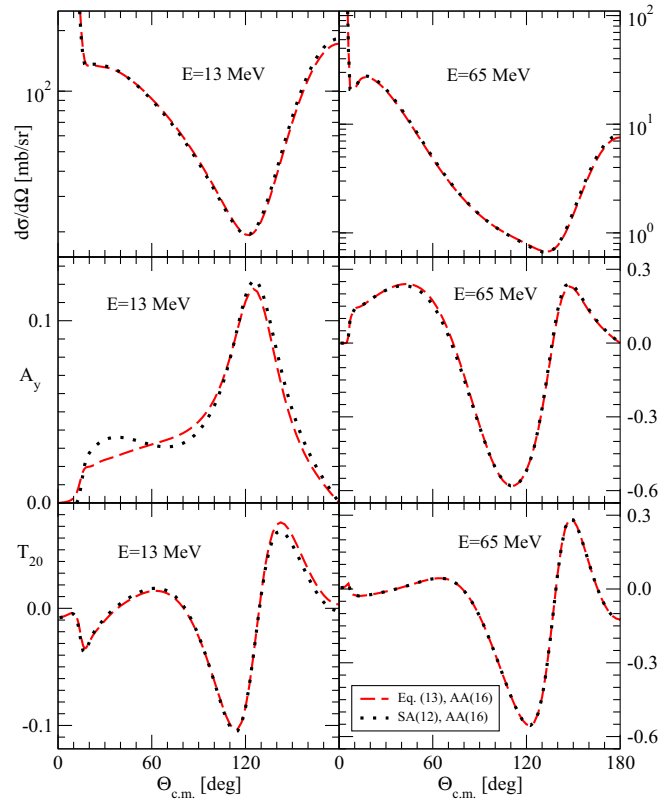

FIG. 3. The predictions for the *pd* elastic scattering cross section $\frac{d\sigma}{d\Omega}$, proton analyzing power A_y, and the deuteron tensor analyzing power T_{20}, shown as a function of the c.m. angle $\Theta_{\rm c.m.}$ at the incoming laboratory proton energy $E = 13$ and 65 MeV. The black dotted lines show results of our SA(12) approach and the red dashed lines of the approach based on Eq. (13). In both cases the elastic scattering transition amplitude AA(16) was used. These observables were calculated with the screened Coulomb force ($R = 40$ fm, $n = 4$) and the AV18 nucleon-nucleon potential [26] restricted to the $j \leqslant 3$ partial waves.

radius R, are compared with the *nd* angular distributions at the incoming proton or neutron laboratory energies $E = 10$, 65, 135, and 250 MeV. On the scale of the figure the *pd* cross sections for all screening radii R are practically indistinguishable with the exception of forward c.m. angles below $\approx 30^\circ$, shown in insets. At very forward angles cross sections for $R = 5$ and 10 fm clearly deviate, but starting from $R = 40$ fm the screening limit is achieved, with the exception of $E = 10$ MeV, which requires at forward angles even larger values of R. We checked that the same picture of approaching the screening limit is seen for all other elastic scattering spin observables (altogether 55 observables, including proton analyzing power, deuteron vector and tensor analyzing powers, spin correlation coefficients, as well as spin transfer coefficients from the nucleon or deuteron to the nucleon or deuteron). The achieved screening limit for a particular observable is equal to the prediction for that observable obtained with the limiting off-shell three-dimensional Coulomb t-matrix of Eq. (19) (brown solid lines in Fig. 2), which is a very strong test of reaching the screening limit.

At $E = 13$ and 65 MeV we compared results of the SA(12) approach to that of Eq. (13), taking the limiting screening value of $R = 40$ fm. In Fig. 3 the predictions for the cross section, proton analyzing power A_y, and the deuteron tensor analyzing power T_{20}, of the first approach [SA(12), the black dotted line] and second approach [Eq. (13), the red dashed line) are shown. There is a nice agreement between predictions of both approaches at $E = 65$ MeV, which extends also to other, not shown, observables. At $E = 13$ MeV for some spin observables, like A_y shown in Fig. 3, differences appear, but generally also here the agreement is good. These results demonstrate that, even with such a rather small $j \leqslant 3$ basis, cancellation effects cause our simplified approach to work quite well.

The basic difference between these two approaches lies in the treatment of the first pair of contributing Coulomb terms in Eq. (11): namely the term with the three-dimensional Coulomb t-matrix $\langle pq\alpha|t^R_{N+c}PG_0t^R_cP|\Phi\rangle$ and its partial-wave decomposed counterpart $-\langle pq\alpha|t^R_{N+c}PG_0\sum_{\alpha'}\int|\alpha'\rangle\langle\alpha'|t^R_cP|\Phi\rangle$. While the SA(12) approach relies solely on the cancellation of contributions of these terms, in the second one, based on Eq. (13), they are calculated explicitly. Since one expects

that the magnitude of the Coulomb terms as well as of the Coulomb force effects diminishes with increasing energy, the above mentioned differences at 13 MeV could be interpreted as a warning that one should avoid a direct calculation of complicated terms containing a three-dimensional Coulomb t-matrix and, instead, rely on the cancellation between contributing Coulomb terms. Presently the terms with a three-dimensional Coulomb t-matrix can be calculated only for very restricted sets of partial-wave states $|\alpha\rangle$ and total 3N angular momenta J, highly insufficient in full-fledged calculations needed for analyses of data.

In the following we concentrate on the SA(12) approach, showing how its precision can be improved and performance controlled. It is evident that increasing the number of partial-wave states $|\alpha\rangle$ would strengthen the cancellation effect between contributing Coulomb terms, improving thus approximation SA(12). Namely, for any particular value of the screening radius R there is a finite number of partial-wave states which reproduce exactly the three-dimensional Coulomb t-matrix. In the extreme case when $|\alpha\rangle$ is taken as such a set of states, the Coulomb terms in the Faddeev equation (11) cancel exactly and the approach based on SA(12) becomes an exact one. Otherwise it is only an approximation, the quality of which depends on how large the cancellation effect is between Coulomb terms. Since that cancellation concerns not only Coulomb terms in Eq. (11) but also to some extent those in elastic scattering and breakup transition amplitudes of Eqs. (15)–(16), the condition reflecting degree of cancellation can be made quantitative by comparing cross sections (observables) obtained with only the first term and with all terms in Eqs. (15)–(16). In the case of a complete cancellation they should be equal. However, in many cases it will be sufficient when these two results converge with an increasing basis $|\alpha\rangle$ even to different values. Starting from an initial set of $|\alpha\rangle$ states one needs to extend it by incorporating consecutive states from $|\beta\rangle$.

To study this in more detail we extended the set of $|\alpha\rangle$ states by adding to the initially chosen states with $j \leqslant j_s = 3$, in which both strong interactions and pp Coulomb force act, some partial-wave states from set $|\beta\rangle$ with $j_s \leqslant j \leqslant j_{\max}$, in which only pp Coulomb force operates. In the following such an extended set of $|\alpha\rangle$states will be denoted by "$jsj_sjj_{\max}$," so that the initially used set is denoted by $js3j3$. We solved SA(12) at $E = 10$ MeV for a number of extended $|\alpha\rangle$ sets: $js3j5$, $js3j7$, $js3j8$, $js3j9$, and $js3j10$, and looked for a pattern of convergence for different elastic scattering observables with a growing number of $j_{\max}$. The increase in number of treated partial waves for given total angular momentum J and parity π of the ppn system is large and amounts to 89 for $js3j3$, 165 for $js3j5$, and 539 for $js3j10$. In spite of that increase the time required to solve numerically Faddeev equations remains restricted due to the fact that partial waves of pure Coulomb nature $|\beta\rangle$ (with $j_s \leqslant j \leqslant j_{\max}$) do not couple between themselves (see a remark about the third term after (10) and Eq. (2) in Ref. [9]).

We found for practically all elastic scattering observables that the convergence in $j_{\max}$ is rapid. The ones most influenced by changes of $j_{\max}$ are low energy proton and deuteron vector analyzing powers, A_y and iT_{11}, which require for converged result at 10 MeV the basis $js3j7$. At 65 MeV and higher energies it is sufficient to use the basis $js3j3$, which reflects the diminishing pp Coulomb force effects for higher energies.

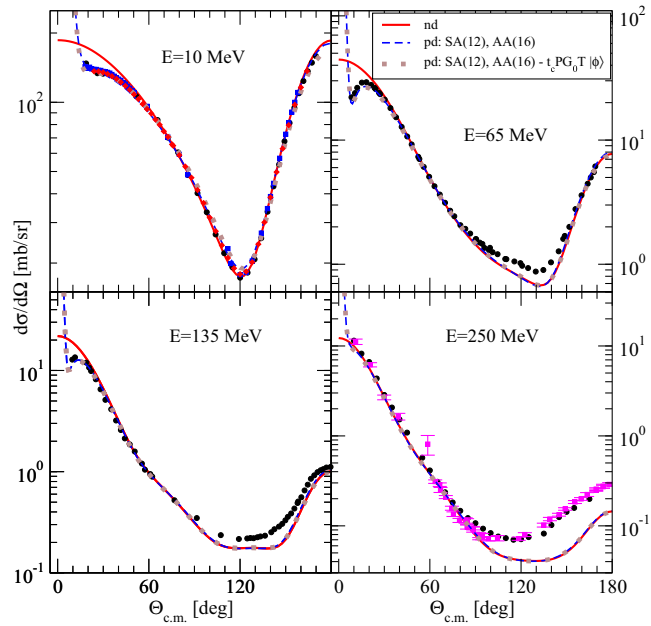

FIG. 4. Comparison of data and predictions for the pd elastic scattering cross section $\frac{d\sigma}{d\Omega}$ obtained in SA(12) and using elastic scattering transition amplitude AA(16), at the incoming proton laboratory energy $E = 10, 65, 135$, and 250 MeV. The cross sections were calculated with the screened Coulomb force ($R = 40$ fm, $n = 4$) and the AV18 nucleon-nucleon potential [26] restricted to the $j \leqslant 3$ partial waves. The pure Coulomb term $\langle\Phi'|Pt_cP|\Phi\rangle$ was determined with the three-dimensional Coulomb t-matrix t_c according to Eq. (19) (blue dashed line). At $E = 10$ MeV the set $js3j7$ of $|\alpha\rangle$-states was used while for other energies the set $js3j3$. The red solid line is the corresponding nd elastic scattering cross section. The brown dotted lines show the results when also the fourth term in (15) $(-\langle\vec{p}\vec{q}\,|\sum_{\alpha'}\int|\alpha'\rangle\langle\alpha'|t_c^R PG_0\sum_{\alpha''}\int|\alpha''\rangle\langle\alpha''|T|\Phi\rangle)$ is included in elastic scattering transition amplitude AA(16). The black circles, blue squares and red diamonds at $E = 10$ MeV are pd elastic scattering cross section data of Refs. [27–29], respectively. The black circles at $E = 65$ MeV are pd data from [30], at $E = 135$ MeV from [31], and at $E = 250$ MeV from [32]. The magenta squares at $E = 250$ MeV are nd data from [33].

In Figs. 4–7 we compare at different energies pd predictions of the SA(12) approach, using elastic scattering amplitude AA(16) with the screening radius $R = 40$ fm and calculating the Coulomb term $\langle\Phi'|Pt_c^R P|\Phi\rangle$ with the limiting three-dimensional off-shell Coulomb t-matrix of Eq. (19), to available pd data for the elastic scattering cross section (Fig. 4), the deuteron vector analyzing power iT_{11} (Fig. 5), the proton analyzing power A_y (Fig. 6), and the deuteron tensor analyzing power T_{20} (Fig. 7). To emphasise the importance and magnitude of Coulomb effects we provide also nd predictions for these observables. Large pp Coulomb force effects for elastic scattering observables are concentrated mainly at forward angles below $\theta_{\text{c.m.}} \approx 30^\circ$ and they diminish with increasing energy. For the cross section the characteristic pattern caused by the pp Coulomb force is properly reproduced by

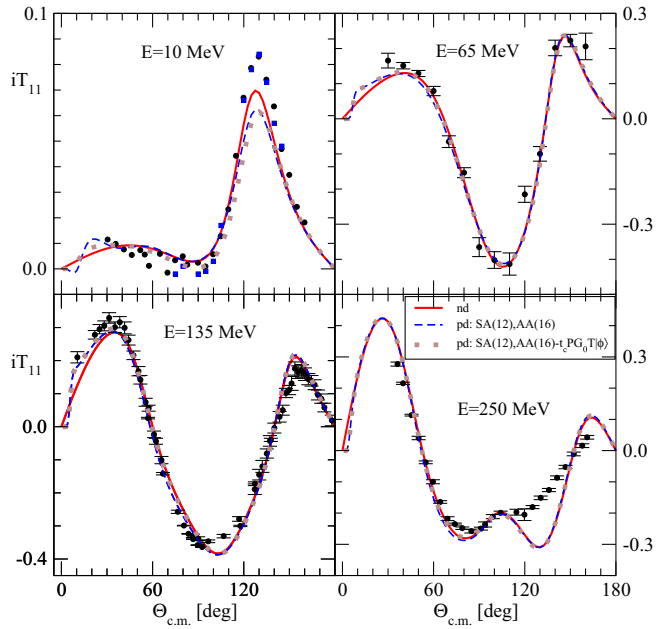

FIG. 5. The same as in Fig. 4 but for the deuteron vector analyzing power iT_{11}. For the description of lines see Fig. 4. The black circles are *pd* data from [34] at $E = 10$ MeV, [35] at $E = 65$ MeV, [36] at $E = 135$ MeV, and [37] at $E = 250$ MeV. The blue squares at $E = 10$ MeV are *pd* data from [38].

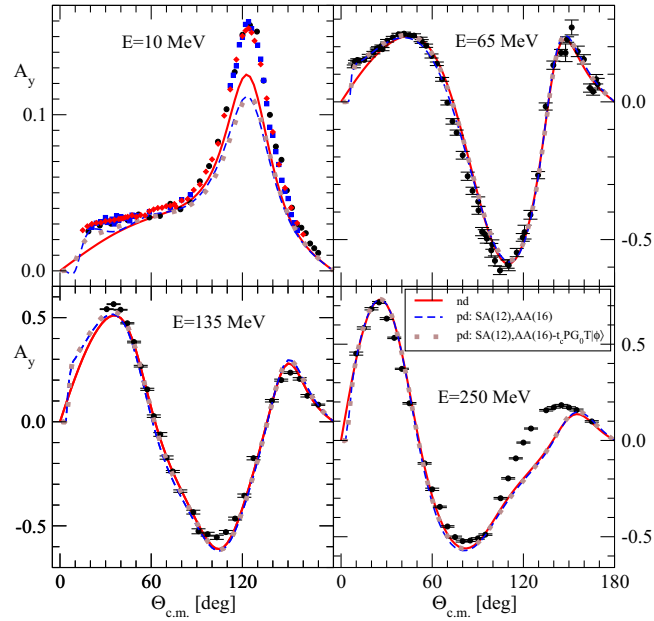

FIG. 6. The same as in Fig. 4 but for the proton analyzing power A_y. For the description of lines see Fig. 4. The black circles are *pd* data from [34] at $E = 10$ MeV, [30] at $E = 65$ MeV, [39] at $E = 135$ MeV, and [32] at $E = 250$ MeV. The blue squares at $E = 10$ MeV are *pd* data from [28] and red diamonds are from [29].

the calculations. Also the forward angle data for A_y, iT_{11}, and T_{20} are nicely reproduced. It follows that large discrepancies between *pd* cross section data and predictions at middle and backward c.m. angles, which grow with increasing energy, are not caused by the *pp* Coulomb force and must be explained either by the action of three-nucleon forces (3NFs) ($E = 65$ and 135 MeV) [40] or through activation of mesonic degrees of freedom ($E = 250$ MeV) [41].

The above results were obtained omitting completely the second pair of Coulomb terms, namely the fourth and fifth terms, in the exact elastic scattering transition amplitude EA(15). To answer the question of how the elastic scattering observables are affected by approximation AA(16) for the scattering amplitude, numerical calculations of both neglected terms are required. The computation of the first term, $-\langle\vec{p}\vec{q}|\sum_{\alpha'}\int|\alpha'\rangle\langle\alpha'|t_c^R PG_0\sum_{\alpha''}\int|\alpha''\rangle\langle\alpha''|T|\Phi\rangle$, is straightforward, but determination of the second one, $\langle\vec{p}\vec{q}|t_c^R PG_0\sum_{\alpha'}\int|\alpha'\rangle\langle\alpha'|T|\Phi\rangle$, which contains the three-dimensional Coulomb t-matrix t_c^R, presents quite a formidable numerical task according to expressions (D.9), (D.6), and (D.8) of Ref. [11]. We postpone direct numerical calculation of this term till a future study and here we would like to present some plausible arguments which justify omission of both terms for AA(16) for elastic scattering at energies considered in the present study. To that end we investigated changes of elastic scattering observables induced by inclusion of the first term in the calculation of observables at our four energies with $js3j3$ set $|\alpha\rangle$. It turned out that at $E = 65$, 135, and 250 MeV the modifications are practically negligible for all 55 elastic scattering observables. At the lowest investigated energy $E = 10$ MeV, some spin observables were modified by ≈5–10 %. Changing the set $js3j3$ to $js3j7$ led to a similar picture at 10 MeV. In Figs. 4–7 we display using brown dotted lines predictions obtained with the term $-\langle\vec{p}\vec{q}|\sum_{\alpha'}\int|\alpha'\rangle\langle\alpha'|t_c^R PG_0\sum_{\alpha''}\int|\alpha''\rangle\langle\alpha''|T|\Phi\rangle$ included in

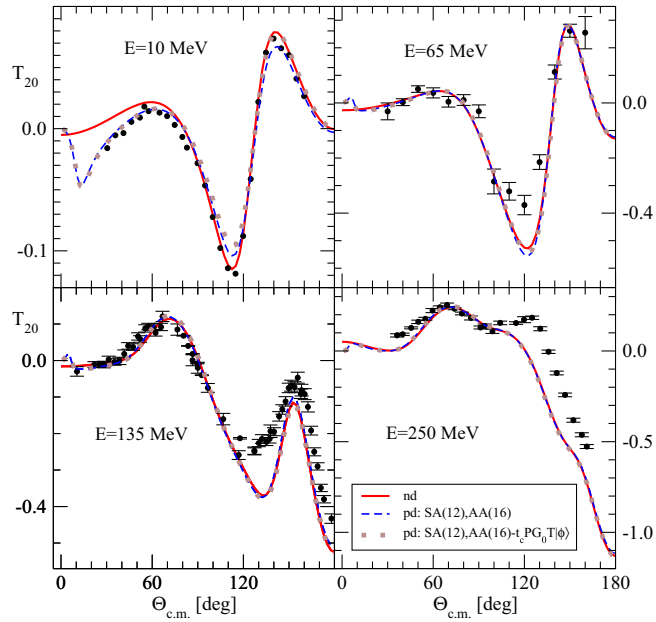

FIG. 7. The same as in Fig. 4 but for the deuteron tensor analyzing power T_{20}. For the description of lines see Fig. 4. The black circles are *pd* data from [38] at $E = 10$ MeV, [35] at $E = 65$ MeV, [36] at $E = 135$ MeV, and [37] at $E = 250$ MeV.

AA(16). It permits us to conclude that the magnitude of this term diminishes with the increasing energy and at the higher energies this term can be safely dropped. At the lowest energy studied (10 MeV) its contribution is not overwhelmingly large. That, together with the fact that also in exact elastic scattering amplitude EA(15) one expects a cancellation between contributions from the second pair of the Coulomb terms similar to that for the first pair, seems to justify the omission of the two terms discussed.

B. Breakup reaction

The exclusive breakup reaction offers a rich spectrum of kinematically complete geometries with observables sensitive to underlying dynamics. We decided to focus on three geometries specified by a kinematical condition for momenta of the three outgoing nucleons. In the so-called final-state-interaction (FSI) geometry the two outgoing nucleons have equal momenta. In neutron-deuteron (nd) breakup their strong interaction in the $^1S_0$ state leads to a characteristic cross section maximum occurring at the exact FSI condition, the magnitude of which is sensitive to the $^1S_0$ scattering length. In the symmetrical-space-star (SST) configuration the momenta of the three outgoing nucleons in the 3N center of mass (c.m.) have the same magnitudes and form a three-pointed "Mercedes-Benz" star. That star lies in a plane inclined under an angle α with respect to the beam direction with momenta of the two outgoing and detected nucleons (in our case protons) lying symmetrically to the beam. The quasi-free-scattering (QFS) geometry refers to a situation where one of the nucleons is at rest in the laboratory system. In pd breakup the np or pp QFS configurations are possible, while for nd breakup np or neutron-neutron (nn) quasifreely scattered pairs can emerge.

The characteristic feature of the exact approach of Refs. [11,12] as well as of our simplified one is the appearance in the breakup transition amplitude of a new term, $\langle \vec{p}_0\vec{q}|(1+P)t_c^R P|\Phi\rangle$, based on a three-dimensional Coulomb t-matrix, t_c^R, analogous to the Rurherford term in the elastic pd scattering. The expression for this term given in Appendix C of Ref. [11] [Eq. (C.3)] shows that the largest contributions from this term are expected in the region of the breakup phase space where the argument of the deuteron wave function, $\varphi_L(|\vec{q}+\frac{1}{2}\vec{q}_0|)$, vanishes. That condition $\vec{q}=-\frac{1}{2}\vec{q}_0$ occurs in the pp QFS, where the spectator neutron rests in the laboratory system (see also the discussion on p. 185 of Ref. [5]). Therefore one expects large pp Coulomb force effects for that geometry. Also large Coulomb effects are expected in the pp FSI region, where two outgoing protons have equal momenta and interact strongly. For nn FSI this leads to a pronounced cross section maximum just at the nn FSI condition and in the case of pp FSI the Coulomb barrier should prevent such a maximum from forming.

In the following we start to investigate the breakup reaction using simplified approach SA(12) with the set $js3j3$ and the breakup transition amplitude AA(16). First we demonstrate the pattern of convergence to the screening limit in two exclusive geometries, QFS as well as FSI, and show that the final results do not depend on how specifically the on-shell breakup amplitudes, which undergo renormalization, are derived. We will apply renormalization to the on-shell breakup amplitudes obtained in two different ways. In the first approach the on-shell breakup amplitudes $\langle p_0 q\alpha|T^R|\Phi\rangle$ ($\langle p_0 q\alpha|t_c^R P|\Phi\rangle$) are obtained by interpolation from the off-shell ones $\langle pq\alpha|T^R|\Phi\rangle$ ($\langle pq\alpha|t_c^R P|\Phi\rangle$) (ONSH1), with subsequent removal of the oscillating phase factor $e^{i\Phi_n^R}$ when calculating the breakup transition amplitude. In the second method we generate the half-shell pp t-matrix $t^R_{N+c}(p_0,p';E-\frac{3}{4m}q^2)$ $[t_c^R(p_0,p';E-\frac{3}{4m}q^2)]$ and calculate the on-shell transition matrix elements $\langle p_0 q\alpha|T^R|\Phi\rangle$ $[\langle p_0 q\alpha|t_c^R P|\Phi\rangle]$ according to Eq. (12) (ONSH2). Here one has to use unrenormalized $t^R_{N+c}(p_0,p';E-\frac{3}{4m}q^2)$ $[t_c^R(p_0,p';E-\frac{3}{4m}q^2)]$ and postpone again the renormalization to calculation of the breakup transition amplitude.

In Fig. 8 we present the pattern of convergence in the screening radius R for the pp QFS. Taking unrenormalized on-shell breakup amplitudes obtained by an interpolation from the off-shell solutions of the Faddeev equations to the on-shell values (p_0,q) (ONSH1) provides unrenormalized pp QFS cross sections which change with varying R [Fig. 8(a)]. Renormalizing these amplitudes stabilizes the cross sections for the screening radii $R \geqslant 20$ fm [see Fig. 8(b)]. The limiting values of the pp QFS cross sections do not depend on the way the on-shell breakup amplitudes are determined [see Figs. 8(b) (ONSH1) and 8(c) (ONSH2)]. These two methods lead to the same final pp QFS cross sections. That the screening limit has been achieved is confirmed in Fig. 8(b), where the violet dotted line shows the result for $R=40$ fm with the pure Coulomb term $\langle \vec{p}_0\vec{q}|(1+P)t_c P|\Phi\rangle$ determined using the final three-dimensional Coulomb t-matrix of Eq. (24).

In Fig. 9 we present analogous investigation for the pp FSI configuration. The large effect of the pp Coulomb force is seen in the region of FSI where, instead of a clear maximum present for nn FSI, the cross section is reduced practically to zero by the pp Coulomb barrier. The pattern of approaching the limiting value is similar to the case of the pp QFS, and final result also here does not depend on how the on-shell breakup amplitudes were derived. To get the final values of the cross section one needs to go to a larger screening radius than in the case of the pp QFS [see Fig. 9(b)].

In Fig. 8 non-negligible effects of renormalization [Figs. 8(a) and 8(b)], which raise the cross section by $\approx$5% in the maximum, are seen for that particular pp QFS configuration. In order to investigate the renormalization as well as the pp Coulomb force effects for all pp QFS configurations, we looked at the pp quasi-free-scattering cross section exactly at the QFS condition (maximum of the cross section) as a function of the laboratory angle of the first outgoing proton $\theta_1^{\text{lab.}}$ $[d(p,p_1p_2)n]$. Since later we will compare theoretical predictions to available pp QFS cross section data at $E=9.5$, 13, 19, 22.7, and 65 MeV, we show in Fig. 10 results of this investigation for three energies: $E=13$, 19, and 65 MeV. At each energy at given $\theta_1^{\text{lab.}}$ there are 2 solutions for the QFS condition, the second one (upper branch in Fig. 10) corresponding to small values of the angle $\theta_2^{\text{lab.}}$ and energy $E_1^{\text{lab.}}$. The full result with renormalization is given by the

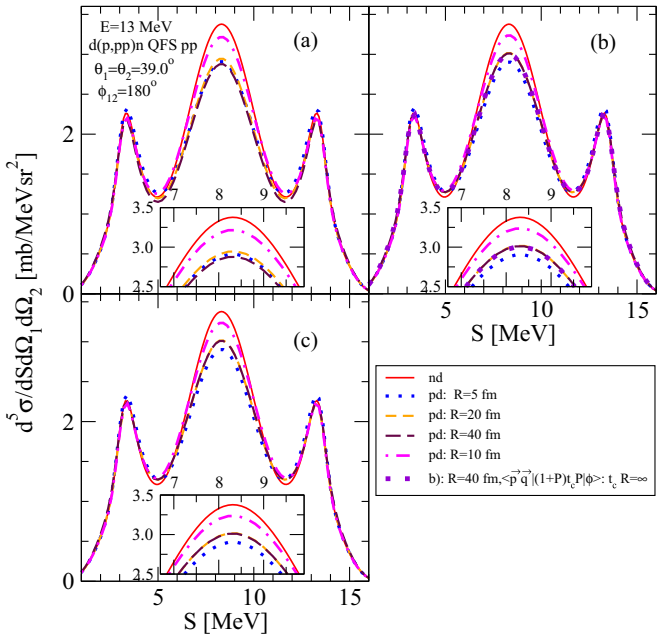

FIG. 8. The convergence with respect to the cutoff radius R of the pd breakup cross section $\frac{d^5\sigma}{d\Omega_1 d\Omega_2 dS}$ shown as a function of the S-curve length for the pp QFS kinematically complete configuration at the incoming proton laboratory energy $E = 13$ MeV. The screening radii are ($n = 4$) $R = 5$ fm (blue dotted line), $R = 10$ fm (magenta dashed-dotted line), $R = 20$ fm (orange short-dashed line), $R = 40$ fm (maroon long-dashed line). These cross sections were calculated using approach SA(12) with the screened Coulomb force and the AV18 nucleon-nucleon potential [26] restricted to the $j \leqslant 3$ partial waves (set $js3j3$), taking the on-shell Faddeev amplitudes AA(16) obtained in two different ways and applying renormalization when calculating the breakup transition amplitude. In (a) unrenormalized on-shell amplitudes gained by interpolation from the off-shell ones were used (ONSH1). In (b) the on-shell amplitudes of (a) have been renormalized before calculating observables. In (c) the on-shell amplitudes were calculated according to (12) (ONSH2) with the unrenormalized pp part of t^R_{N+c} (t^R_c) and renormalization was performed before calculating observables. The red solid line is the corresponding nd elastic scattering cross section. The violet dotted line in (b) is the result with $R = 40$ fm but with the pure Coulomb term $\langle \vec{p}_0\vec{q}|(1+P)t^R_c P|\Phi\rangle$ determined with the screening limit for t^R_c given by Eq. (24).

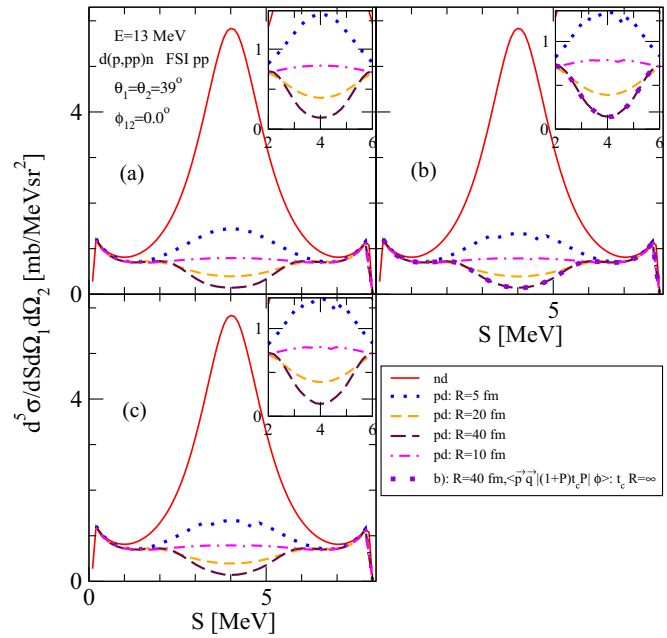

FIG. 9. The same as in Fig. 8 but for the pp FSI kinematically complete configuration.

blue long-dashed line, which compared with the green dotted line (without renormalization) reveals the importance and the magnitude of renormalization. The non-negligible renormalization effects at $E = 13$ MeV of the order of ≈5–8% are seen only for $\theta_1^{\text{lab.}} \in (10^\circ, 50^\circ)$. At 19 and 65 MeV the renormalization causes in pp QFS only insignificant effects.

In order to get the information of the Coulomb force effects in Fig. 10 also the nd prediction is shown by the solid red line. The Coulomb effects are largest at $E = 13$ MeV as evidenced by the nd results as well as by the maroon dotted line, resulting when the term with the three-dimensional Coulomb t-matrix, $\langle \vec{p}_0\vec{q}|(1+P)t^R_c P|\Phi\rangle$, is omitted in AA(16), or by the magenta dashed-dotted line, resulting when both Coulomb terms, the one above and $-\langle \vec{p}_0\vec{q}|(1+P)\sum_{\alpha'}\int|\alpha'\rangle\langle\alpha'|t^R_c P|\Phi\rangle$, are absent in AA(16). The Coulomb effects diminish rapidly with growing energy, becoming practically negligible at 65 MeV, with the exception of forward angles $\theta_1^{\text{lab.}}$ and $\theta_2^{\text{lab.}}$ on lower and upper branches, respectively. It is interesting to note that the angular dependence of the pp QFS cross section resembles that of pd elastic scattering, with the characteristic increase at forward angles caused by the Coulomb term $\langle \vec{p}_0\vec{q}|(1+P)t^R_c P|\Phi\rangle$. Also the importance and magnitude of the Coulomb force effects in pp QFS resembles those in a free pp scattering (see insets in Fig. 10). To exemplify the cancellation effect between the Coulomb terms in the pp QFS breakup transition amplitude we show in Fig. 10 also cross sections (black double-dotted-dashed line) obtained with these two terms only. In the region of angles $\theta_1^{\text{lab.}} \in (10^\circ, 40^\circ)$ the resulting values of that cross section are about $\approx 10^{-1}$ mb/(MeV sr^2) for that set of $|\alpha\rangle$ states, which illustrates quite significant cancellation, although not as large as for the case of the pp FSI or pd SST (see below).

In Figs. 11 and 12 results of a similar investigation are shown for pp FSI and pd SST, respectively. The action of the Coulomb barrier brings the pp FSI cross section close to zero for all pp FSI configurations. Regardless of their production angle $\theta_1^{\text{lab.}}$, the renormalization effect is insignificant and the cancellation between two contributing Coulomb terms appears drastic (black double-dotted-dashed line). The pp FSI cross section is determined practically by only the first term $\langle \vec{p}_0\vec{q}|(1+P)\sum_{\alpha'}\int|\alpha'\rangle\langle\alpha'|T|\Phi\rangle$ in the breakup transition amplitude AA(16). For the SST configurations the largest effects of renormalization as well as of the pp Coulomb force are present at $E = 13$ and 19 MeV around $\alpha_{\text{c.m.}} \approx 40^\circ$. They become again negligible at $E = 65$ MeV. When the star plane is perpendicular to the beam direction the renormalization

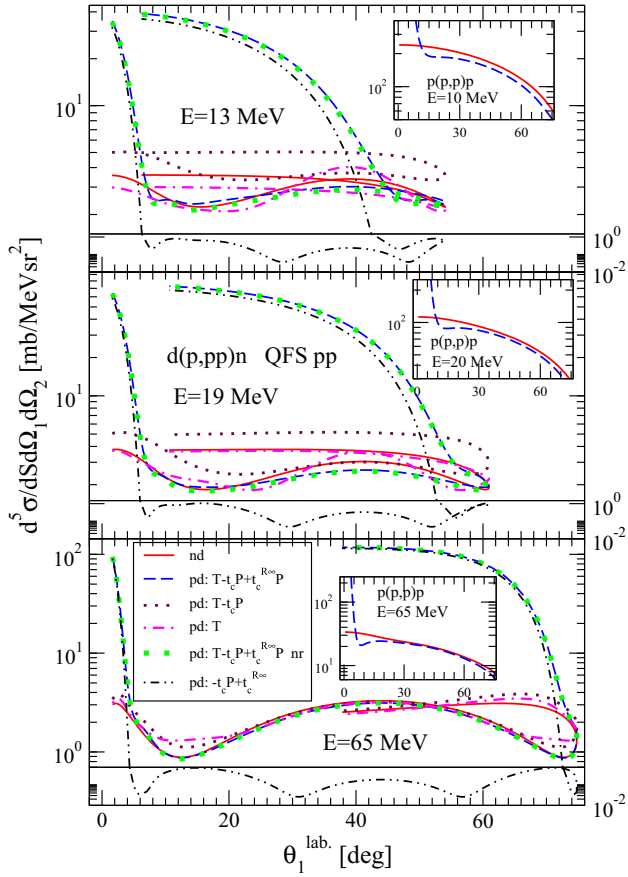

FIG. 10. The *pd* breakup $d(p,pp)n$ cross section calculated at the *pp* QFS condition for the incoming proton laboratory energies $E = 13$, 19, and 65 MeV, as a function of the angle of the outgoing proton 1. The SA(12) approach with set of $js3j3$ partial waves and the screening radius $R = 40$ fm ($n = 4$) was used, with on-shell AA(16) Faddeev amplitudes obtained by an interpolation from the off-shell ones (ONSH1), renormalized before calculating observables. The pure Coulomb term $\langle \vec{p}_0\vec{q}|(1+P)t_c^R P|\Phi\rangle$ in AA(16) was determined with the screening limit for t_c^R given by Eq. (24). The blue long-dashed line is the result with all three terms in AA(16). Also the result of AA(16) without renormalization (nr) is shown by the green dotted line. The maroon dotted and magenta dashed-dotted lines follow when the term with three-dimensional t_c^R Coulomb t-matrix and both terms with t_c^R, respectively, are omitted, and the black double-dotted-dashed line shows the result when only these two terms are kept. At the bottom of each figure the continuation of the black double-dotted-dashed line is shown in a compressed y-axis scale shown on the right side. The red solid line is the *nd* breakup cross section. In insets the laboratory cross sections $d\sigma/d\Omega$ ($\frac{mb}{sr}$) for *pp* scattering at laboratory energies $E = 10$, 20, and 65 MeV are shown as a function of the proton laboratory angle. Here the red solid and blue dashed lines are the AV18 cross sections without and with *pp* Coulomb interaction, respectively.

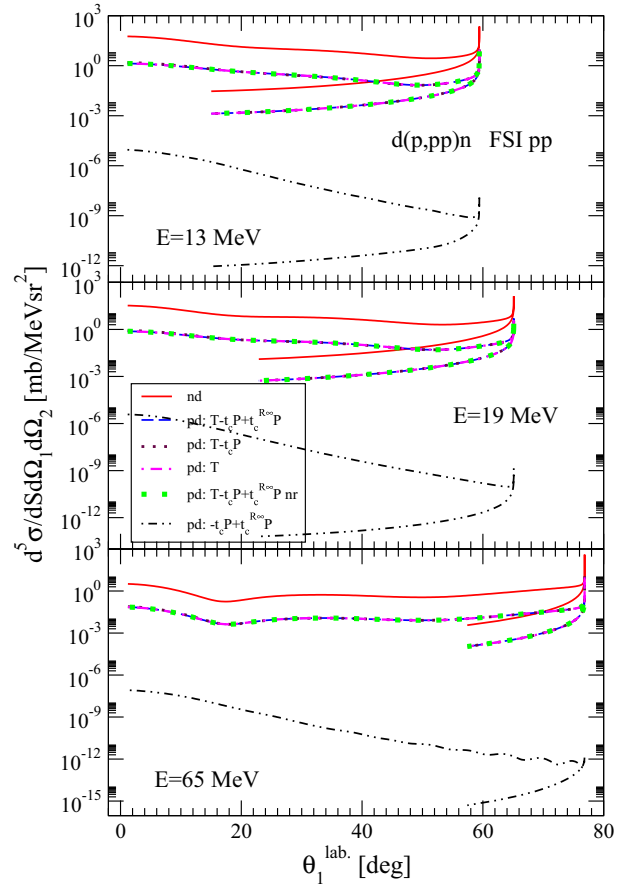

FIG. 11. The same as in Fig. 10 but for the *pd* breakup $d(p,pp)n$ cross section $d^5\sigma/d\Omega_1 d\Omega_2 dS$ calculated at the *pp* FSI condition ($\vec{p}_1 = \vec{p}_2$).

effects are small. As for the *pp* FSI, the cancellation effects in the breakup transition amplitude for that configuration are very large.

In Figs. 13 and 14 we show examples of comparison of our theoretical predictions to *pd* breakup cross section data at $E = 13$ and 65 MeV for SST ($\alpha_{\text{c.m.}} = 90^\circ$) and *pp* QFS configurations. We show predictions of our simplified approach SA(12) (blue short-dashed line) and of the approach based on Eq. (13) (maroon dotted line). At 13 MeV they agree very well with each other for *pp* QFS, differing by ≈10% for SST. Both disagree significantly with the *pd* SST cross section data, underestimating slightly *pp* QFS data. At 65 MeV they are close to each other and agree quite well with the SST data, differing again only slightly from the *pp* QFS data. This is similar to what we have found for elastic scattering when comparing these two approaches, and seems to support the validity of the assumption about the cancellation of the Coulomb terms in our simplified approach SA(12), at the same time indicating that using directly computed complex terms with three-dimensional Coulomb t-matrix is hazardous.

In Ref. [47] a correct description of the low energy pp QFS cross section data was reported. That prompted us to reanalyze available low energy *pp* QFS cross section data and look for a possible reason of the slight discrepancy found at 13 MeV in Fig. 13. In Fig. 15 we compare $E = 19$ MeV data of Refs. [45,46] and $E = 22.7$ MeV data of Ref. [44] to our theoretical predictions SA(12), obtained with the renormalized and unrenormalized $js3j3$ on-shell breakup amplitudes AA(16), received by interpolation from the off-shell ones

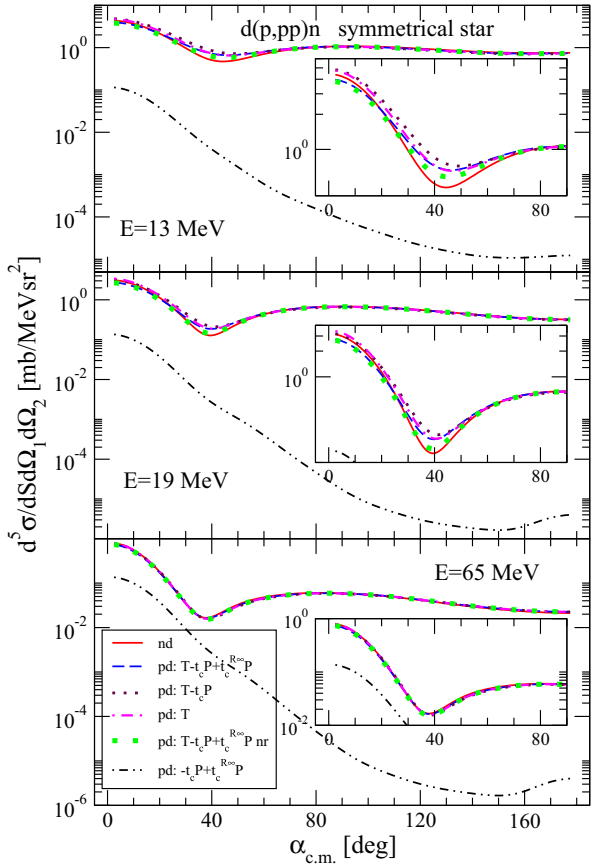

FIG. 12. The same as in Fig. 10 but for the *pd* breakup $d(p, pp)n$ cross section $d^5\sigma/d\Omega_1 d\Omega_2 dS$ calculated at the symmetrical-space-star condition (in the 3N c.m. system the momenta of the three outgoing nucleons are equal and form a symmetrical three-point star in a plane inclined at an angle $\alpha_{\text{c.m.}}$ with respect to the incoming proton momentum).

(ONSH1) (blue short-dashed and green dotted lines, respectively). The same comparison at $E = 9.5$ and 13 MeV for the data from Ref. [47] and at 13 MeV for the data from Ref. [42], is presented in Fig. 16. To make sure that the screening limit has been achieved we show in both figures by the red dotted lines also the renormalized $R = 40$ fm results obtained with the pure Coulomb term calculated using the three-dimensional Coulomb t-matrix according to (24).

A glance at both figures reveals again that the renormalization effects shrink with the growing energy. While at 9.5 and 13 MeV they are non-negligible and enhance the cross section bringing the theory closer to the data, at 19 and 22.7 MeV they are practically insignificant. It is interesting to notice that large effects of the *pp* Coulomb force at smaller energies have a pattern of contributions changing with *pp* QFS configuration (see the orange dashed-dotted and magenta double-dashed-dotted lines in Fig. 16, which show the results when both Coulomb terms are omitted). At 9.5 and 13 MeV theory slightly underestimates *pp* QFS cross sections in practically all configurations. At 19 MeV theory lies between two available data sets, and at 22.7 MeV the data are clearly overestimated.

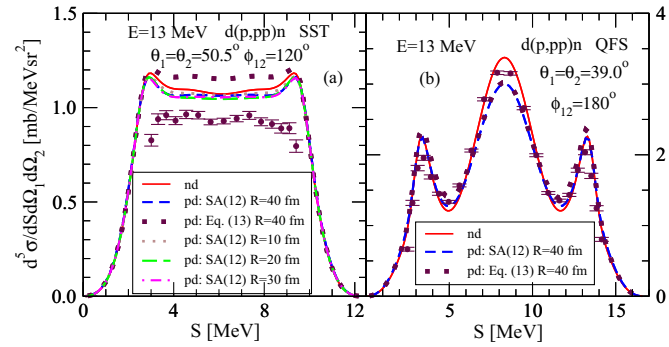

FIG. 13. The *pd* complete breakup $d(p, pp)n$ cross sections $d^5\sigma/d\Omega_1 d\Omega_2 dS$ for the SST and *pp* QFS configurations at 13 MeV of the incoming proton laboratory energy as a function of the arc length of the S curve. They are obtained with the screening radius $R = 40$ fm ($n = 4$) and set $js3j3$ partial waves, using the SA(12) approach (blue short-dashed line) or the approach based on Eq. (13) (maroon dotted line). In both approaches the three-dimensional Coulomb t-matrix t_c is determined according to (24). The on-shell Faddeev amplitudes AA(16) obtained by interpolation from the off-shell ones (ONSH1) are used and renormalized before calculating observables. For SST configuration (a) and the SA(12) approach the convergence in the screening radius R is presented by results with $R = 10$ fm (brown dotted line), $R = 20$ fm (green long-dashed line), and $R = 30$ fm (magenta short-dashed-dotted line). The red solid line is the corresponding *nd* breakup cross section. The maroon circles are *pd* data from Ref. [42].

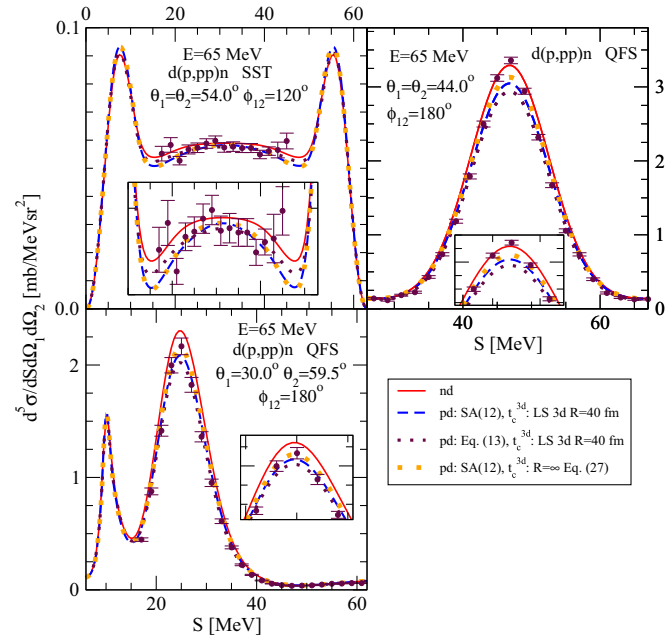

FIG. 14. The same as in Fig. 13 but for the *pd* complete breakup $d(p, pp)n$ cross sections $d^5\sigma/d\Omega_1 d\Omega_2 dS$ in SST and *pp* QFS at 65 MeV. Here in both approaches the three-dimensional Coulomb t-matrix t_c^R was determined by solving the three-dimensional Lippmann-Schwinger equation with the screening radius $R = 40$ fm ($n = 4$). In the case of the SA(12) approach, the effect of using the three-dimensional Coulomb t-matrix t_c determined according to (24) is shown by the orange dotted lines. The maroon circles are *pd* data from Ref. [43].

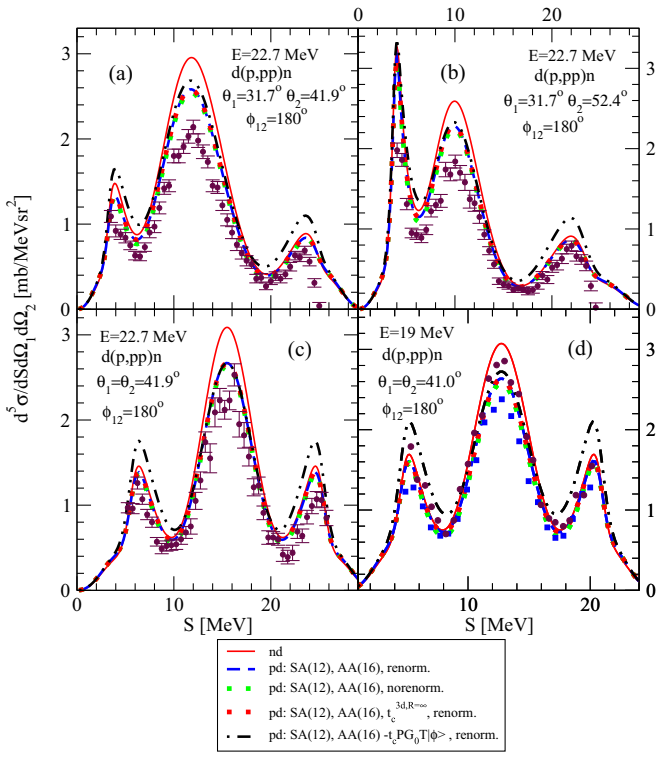

FIG. 15. The *pd* complete breakup $d(p,pp)n$ cross sections $d^5\sigma/d\Omega_1 d\Omega_2 dS$ for *pp* QFS configurations at 22.7 MeV (a)–(c) and 19 MeV (d) of the incoming proton laboratory energy, as a function of the arc length of the S curve. They were obtained with the screening radius $R = 40$ fm ($n = 4$) using the SA(12) approach and set $js3j3$ of partial waves. The on-shell Faddeev amplitudes AA(16) obtained by interpolation from the off-shell ones (ONSH1) were used and renormalized before calculating observables (blue short-dashed line). The green dotted line is a result without renormalization. The black double-dotted-dashed line shows the result when also the fourth term in EA(15) is included in the breakup transition amplitude AA(16). The red dotted line is obtained with the limiting three-dimensional t_c of Eq. (24). The red solid line is the corresponding *nd* breakup cross section. The maroon circles are *pd* data from Ref. [44] for (a)–(c) and from Ref. [45] for (d). The blue squares in (d) are *pd* data from Ref. [46].

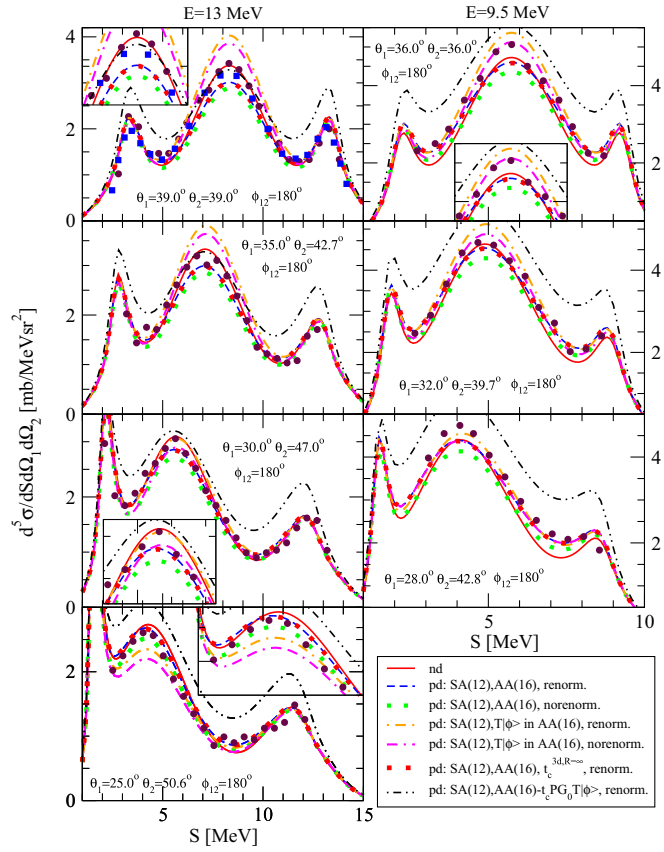

FIG. 16. The same as in Fig. 15 but for the *pp* QFS configurations at 13 and 9.5 MeV. The orange dashed-dotted and magenta double-dashed-dotted lines are renormalized and unrenormalized results, respectively, when both Coulomb terms are omitted in the breakup AA(16). The red solid line is the *nd* breakup cross section. The maroon circles are *pd* data from Ref. [47] and blue squares at 13 MeV are *pd* data from Ref. [28].

The contribution to a particular kinematically complete breakup configuration, specified by momenta of three outgoing nucleons, comes from only three sets (p_i, q_i) of Jacobi-relative-momenta values, belonging to an ellipse of Eq. (20) in the q-p plane. Performing exclusive breakup measurements, one is restricted only to points from that curve, which makes the exclusive breakup reaction a very selective tool. In contrast to the breakup reaction, averaging over the relative momentum of nucleons forming the deuteron causes the elastic *pd* scattering to get contributions from a large region in the q-p plane, which does not overlap with the elliptic curve for the breakup reaction (see Fig. 1 in [48]). It follows that breakup observables should reveal greater sensitivity to the underlying dynamics than elastic *pd* scattering observables. This motivated us to investigate how the extension of the set $|\alpha\rangle$, which has only a small effect on elastic scattering observables, influences the *pp* QFS cross sections.

In Fig. 17 we show the pattern of convergence in partial-wave expansion of the *pp* QFS cross section around QFS point for some *pp* QFS configurations from Fig. 16. The differently colored dashed lines as well as the solid green line are cross sections based on solutions of our SA(12) Faddeev equation with different partial-wave sets and transition amplitude AA(16). The dotted lines show the cross sections resulting when only the first term in AA(16) was kept and the two Coulomb terms were omitted. The same colored lines correspond to the same set of $|\alpha\rangle$ states, with the exception of black dotted and solid green lines, which correspond to the $js3j8$ set. Starting from the set $js3j3$, for which a large effect of omitting the Coulomb terms is seen and a separation between blue the dotted and dashed lines is large, the difference between dashed and dotted lines diminishes rapidly with increasing j and disappears for the $js3j8$ set. Also the dashed lines themselves are converging to the prediction obtained for the set $js3j8$. Including additional partial waves with $j = 9$ and higher does not change the results. It is clear that extending set $|\alpha\rangle$ improves the description of data.

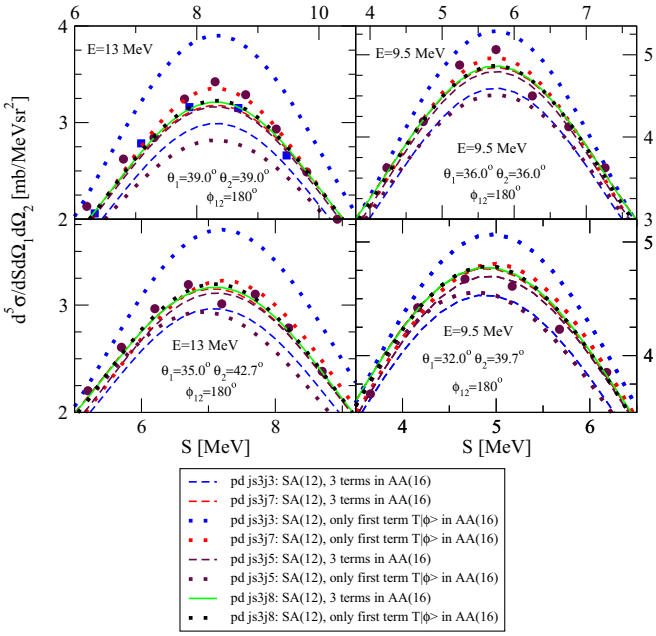

FIG. 17. The pattern of convergence in the sets of partial waves around the QFS *pp* condition for cross sections in chosen configurations from Fig. 16, calculated with the SA(12) approach ($R = 40$ fm, $n = 4$) and the renormalized amplitude AA(16). The meaning of the data symbols is the same as in Fig. 16. Same colored dashed and dotted lines correspond to identical set of partial waves. For dashed lines all three terms in AA(16) contribute to the breakup amplitude while for dotted lines only the first term in AA(16) ($\langle \vec{p}_0\vec{q}|(1+P)\sum_{\alpha'}\int|\alpha'\rangle\langle\alpha'|T|\Phi\rangle$) was taken into account. The sets of partial waves are blue: $js3j3$; maroon: $js3j5$; red: $js3j7$. For the set $js3j8$ the colors of lines are solid green and black dotted for the case when all three terms and only the first one, respectively, were taken into account in AA(16).

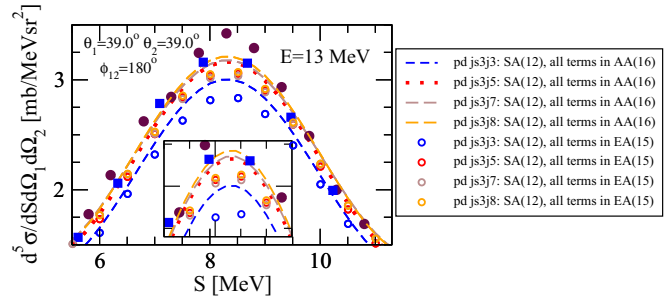

FIG. 18. The pattern of convergence in the sets of partial waves around the QFS *pp* condition for cross section of the first configuration at $E = 13$ MeV from Fig. 16, calculated using the SA(12) approach ($R = 40$ fm, $n = 4$) with the renormalized AA(16) (lines) and EA(15) (circles). The meaning of the data symbols is the same as in Fig. 16. Equally colored lines and circles correspond to identical set of partial waves. For lines all three terms in AA(16) and for circles all five terms in EA(15) contribute to the breakup amplitude. The sets of partial waves are blue (short dashed): $js3j3$; red (dotted): $js3j5$; brown (long dashed): $js3j7$; and orange (long dashed): $js3j8$.

That points to the need for treatment of higher partial waves in breakup, and the convergence of the results shown with the dotted and dashed lines supports our expectation about the stronger cancellation between contributing Coulomb terms with the increasing number of partial waves.

Last but not least, we investigate the significance of the two additional Coulomb contributions to the exact breakup amplitude EA(15) (the fourth and fifth terms) omitted up to now, namely the terms $-\langle\vec{p}\vec{q}|\sum_{\alpha'}\int|\alpha'\rangle\langle\alpha'|t_c^R PG_0\sum_{\alpha''}\int|\alpha''\rangle\langle\alpha''|T|\Phi\rangle$ and $\langle\vec{p}\vec{q}|t_c^R PG_0\sum_{\alpha'}\int|\alpha'\rangle\langle\alpha'|T|\Phi\rangle$. That their contribution can be important is visualized in Figs. 15 and 16, where the black double-dotted-dashed lines show the cross section obtained when in addition to three contributions in AA(16) also the term $-\langle\vec{p}\vec{q}|\sum_{\alpha'}\int|\alpha'\rangle\langle\alpha'|t_c^R PG_0\sum_{\alpha''}\int|\alpha''\rangle\langle\alpha''|T|\Phi\rangle$ was included. The changes of the cross section are quite large at lower energies and become much smaller at 19 and 22.7 MeV, confirming again diminishing of the Coulomb force effects with growing energy. Since changes of the cross section induced by this term are non-negligible, it is unavoidable to include in the transition amplitude also the term with three-dimensional Coulomb t-matrix t_c^R: $\langle\vec{p}\vec{q}|t_c^R PG_0\sum_{\alpha'}\int|\alpha'\rangle\langle\alpha'|T|\Phi\rangle$. One would expect that, similarly as for the first pair of the two Coulomb terms in (15), also terms in the second pair would probably cancel each other when extending the set $|\alpha\rangle$. To check it requires, however, a calculation of this nontrivial modification of the Rutherford term by the strong nucleon-nucleon interactions, as given in Appendix D of Ref. [11] [Eqs. (D.6)–(D.8)]. In Fig. 18 we show the convergence pattern in j for the first *pp* QFS configuration at 13 MeV, where circles represent cross sections obtained with all the five terms included in the exact breakup amplitude EA(15). To facilitate the comparison we also show again by different lines the convergence pattern with three terms in the approximate breakup amplitude AA(16). It is seen that indeed circles converge rapidly to a result which, in the maximum of that *pp* QFS, is ≈5% smaller than the prediction obtained with only the first pair of Coulomb terms in the breakup transition amplitude AA(16). It shows that the two contributions in the second pair of the Coulomb terms of the exact breakup transition amplitude EA(15) do not cancel each other completely in the QFS maximum.

In Figs. 19–21, we show converged results obtained with $js3j8$ set for all herein-investigated *pp* QFS configurations at 9.5 and 13, 19 and 22.7, and 65 MeV, respectively. At 9.5 and 13 MeV the description of data by AA(16) (the green solid line) is significantly improved when compared to $js3j3$ set predictions (the blue short-dashed line). Including in addition the second pair of the Coulomb terms when using EA(15) lowers by ≈5% cross sections in all the QFS maxima, deteriorating slightly the good description of data in that region, leaving it, however, without a change beyond the QFS peak region. At the higher energies the contribution from the second pair of the Coulomb terms in EA(15) becomes insignificant and a nice agreement with data at 19 and 65 MeV is found using AA(16). The large discrepancies compared to data at 22.7 MeV remain.

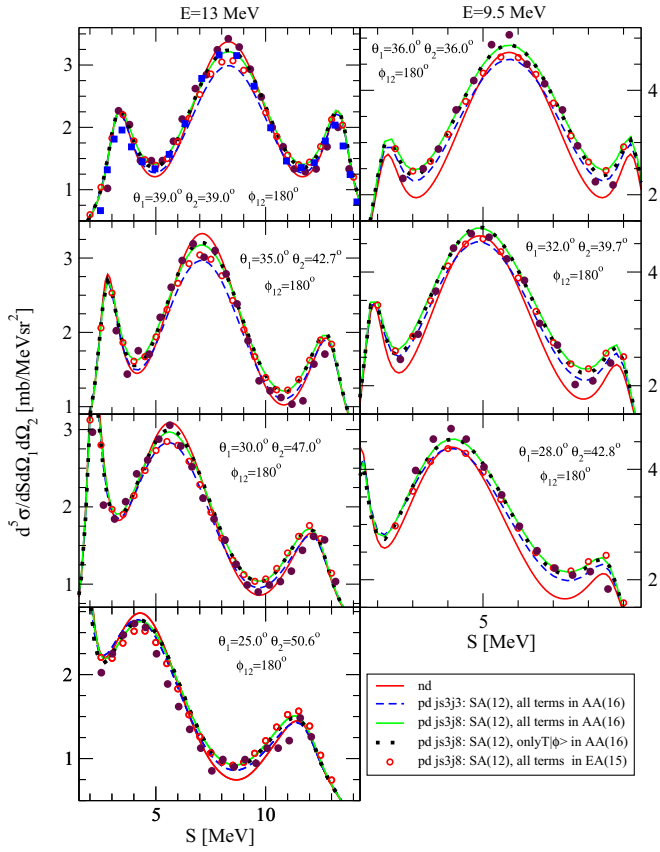

FIG. 19. The *pd* complete breakup $d(p,pp)n$ cross sections $d^5\sigma/d\Omega_1 d\Omega_2 dS$ for the configurations from Fig. 16, calculated using the SA(12) approach and set $js3j8$ of partial waves, with on-shell Faddeev amplitudes obtained by interpolation from the off-shell ones (ONSH1), renormalized before calculating observables. The screening radius $R = 40$ fm ($n = 4$) was used and the green solid lines show the results with all three terms in AA(16) contributing to the breakup amplitude, while for the black dotted lines only the first term in AA(16) was taken into account. The red circles show the cross sections calculated with all five terms in EA(15) included in the breakup amplitude. For the sake of comparison also results with the set $js3j3$ and three terms in AA(16) are shown (the blue short-dashed line). The red solid line is the corresponding *nd* cross section. The meaning of the data symbols is the same as in Fig. 16.

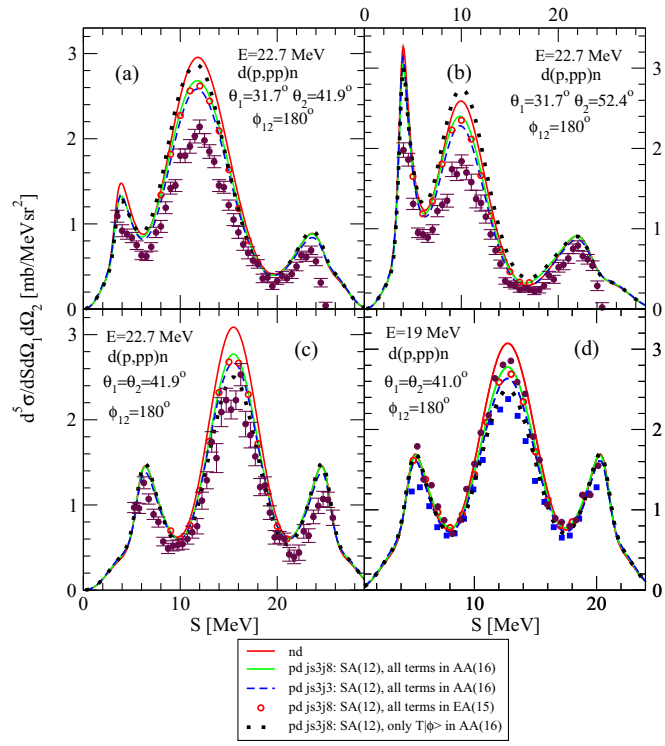

FIG. 20. The same as in Fig. 19 but for the configurations from Fig. 15.

IV. SUMMARY AND CONCLUSIONS

We formulated and applied a simplified approach to the exact treatment of the *pp* Coulomb force in the momentum space 3N Faddeev calculations, presented in Refs. [11] and [12]. That exact treatment is based on a standard formulation for short-range forces and relies on a screening of the long-range Coulomb interaction. It is, however, inconvenient for applications since it contains two contributing terms with a three-dimensional Coulomb t-matrix, which require an unrealistic amount of computer time and resources to compute them in practice. That prevents any application of the exact approach in full-fledged 3N calculations. Our simplified approach contains the main physical ingredients of the exact method but neglects these complex terms altogether, relying on their cancellation. We have applied it in a wide energy range of the incoming proton energies, using the AV18 NN potential to calculate elastic *pd* scattering and breakup observables. The main results are summarized as follows.

(i) We demonstrated and showed numerically that the elastic *pd* scattering amplitude has a well defined screening limit and therefore does not require any renormalization. This is an implication of the fact that only off-shell values of Jacobi momenta and consequently, only off-shell 2N t-matrices are required and enter in the determination of that amplitude. Well

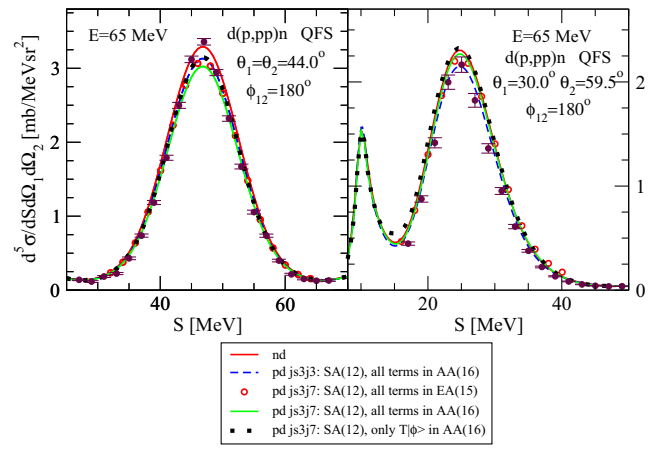

FIG. 21. The same as in Fig. 19 but for the *pp* QFS configurations from Fig. 14.

converged elastic *pd* cross sections and spin observables are obtained at finite screening radii. Additional support for the claim that infinite R limit is achieved, was provided by using directly the limiting analytical expression for the three-dimensional off-shell Coulomb t-matrix when calculating the transition amplitude.

(ii) In contrast to *pd* elastic scattering, for *pd* breakup it is unavoidable to perform renormalization of the breakup amplitudes. The reason is that in breakup only the amplitudes for on-shell values of Jacobi momenta are required, which demands in consequence also half-shell 2N t-matrices. The breakup amplitudes have two contributions, one driven by the interaction in the *pp* subsystem and second by that in the *np* subsystem. Only the first part requires renormalization. We demonstrated that the renormalization has to be performed during calculation of the breakup transition amplitude and the on-shell amplitudes themselves can be derived in two different ways which lead to the same results. We have shown that converged results for breakup can be achieved with finite screening radii. The importance of the renormalization depends on the energy of a 3N system and on the region in the breakup phase-space. It is diminishing with the growing energy, and remains very important at low energies, especially in the region of the QFS condition.

(iii) In our approach to breakup two new terms appear in the scattering amplitude, which to the best of our knowledge have not been discussed before. One corresponds to the Rutherford *pd* Coulomb amplitude in elastic *pd* scattering. This term was found to be important in the region of QFS scattering. Calculating that term with the exact expression for a three-dimensional half-on-shell Coulomb t-matrix provides an additional test that the screening limit for breakup is achieved. The second term is a correction to the first one due to strong interactions between nucleons. We found that its contribution reduces the low energy *pp* QFS cross sections by $\approx 5\%$ in the QFS maximum.

(iv) We have checked the validity of the basic assumption underlying our simplified approach in the case of a restricted basis of partial wave states, for which it was possible to compute the first term with a three-dimensional Coulomb t-matrix in the exact approach. Also results for contributions to the elastic scattering and breakup transition amplitudes, obtained with an extended basis of states, vindicate the cancellation effect between Coulomb terms. The presented results justify using our simplified approach, whose requirements for computer time and resources are comparable to standard *nd* calculations, in future applications. This ensures that the *pp* Coulomb force effects for *pd* reactions can be calculated efficiently and quickly.

(v) We found that large Coulomb force effects are restricted to forward angles for the elastic *pd* scattering and to specific regions of the breakup phase-space. They seem generally to diminish rapidly with the increasing energy of the *pd* system. A comparison to the results published in Ref. [8] proves that our predictions for elastic scattering are very similar. Since one expects that the *pp* Coulomb force effects grow with decreasing energy of the three-nucleon system, a comparison of predictions from both approaches below the deuteron breakup threshold would be very welcome. Such a study is in preparation.

(vi) For breakup reaction inclusion of the *pp* Coulomb force does not help to understand the *pd* space-star cross sections at 13 MeV. Again, predictions of our simplified approach are very similar, both at 13 and 65 MeV, to the results of Ref. [7].

The simplified approach proposed by us can be applied also in the case when in addition to pairwise forces a 3NF contributes to the 3N Hamiltonian. Since the structure of Faddeev equations is very similar an extension to 3N reactions with electromagnetic probes is straightforward.

ACKNOWLEDGMENTS

This research was supported in part by the Excellence Initiative – Research University Program at the Jagiellonian University in Kraków. One of the authors (J.G.) is grateful to Arnoldas Deltuva for helpful discussions. The numerical calculations were partly performed on the supercomputers of the JSC, Jülich, Germany.

[1] E. O. Alt, W. Sandhas, and H. Ziegelmann, Phys. Rev. C **17**, 1981 (1978).
[2] E. O. Alt and W. Sandhas, in *Coulomb Interactions in Nuclear and Atomic Few-Body Collisions*, edited by F. S. Levin and D. Micha (Plenum, New York, 1996), p. 1.
[3] E. O. Alt and M. Rauh, Phys. Rev. C **49**, R2285(R) (1994).
[4] E. O. Alt, A. M. Mukhamedzhanov, M. M. Nishonov, and A. I. Sattarov, Phys. Rev. C **65**, 064613 (2002).
[5] W. Glöckle, H. Witała, D. Hüber, H. Kamada, and J. Golak, Phys. Rep. **274**, 107 (1996).
[6] A. Kievsky, M. Viviani, and S. Rosati, Phys. Rev. C **52**, R15(R) (1995).
[7] A. Deltuva, A. C. Fonseca, and P. U. Sauer, Phys. Rev. C **72**, 054004 (2005).
[8] A. Deltuva, A. C. Fonseca, and P. U. Sauer, Phys. Rev. C **71**, 054005 (2005).
[9] A. Deltuva, A. C. Fonseca, and P. U. Sauer, Phys. Rev. C **73**, 057001 (2006).
[10] E. Stephan *et al.*, Phys. Rev. C **76**, 057001 (2007).
[11] H. Witała, R. Skibiński, J. Golak, and W. Glöckle, Eur. Phys. J. A **41**, 369 (2009).

[12] H. Witała, R. Skibiński, J. Golak, and W. Glöckle, Eur. Phys. J. A **41**, 385 (2009).
[13] A. Deltuva, Phys. Rev. C **110**, 024004 (2024).
[14] H. Witała, W. Glöckle, and H. Kamada, Phys. Rev. C **43**, 1619 (1991).
[15] W. Glöckle, *The Quantum Mechanical Few-Body Problem* (Springer, Berlin, 1983).
[16] J. C. Y. Chen and A. C. Chen, in *Advances of Atomic and Molecular Physics*, edited by D. R. Bates and J. Estermann (Academic Press, New York, 1972), Vol. 8.
[17] L. P. Kok and H. van Haeringen, Phys. Rev. C **21**, 512 (1980).
[18] M. Abramowitz and I. A. Stegun, *Handbook of Mathematical Functions* (Dover, New York, 1972).
[19] R. Skibiński, J. Golak, H. Witała, and W. Glöckle, Eur. Phys. J. A **40**, 215 (2009).
[20] W. F. Ford, Phys. Rev. **133**, B1616 (1964).
[21] W. F. Ford, J. Math. Phys. **7**, 626 (1966).
[22] M. Yamaguchi, H. Kamada, and Y. Koike, Prog. Theor. Phys. **114**, 1323 (2005).
[23] J. R. Taylor, Nuovo Cimento B **23**, 313 (1974).
[24] M. D. Semon and J. R. Taylor, Nuovo Cimento A **26**, 48 (1975).
[25] L. P. Kok and H. van Haeringen, Phys. Rev. Lett. **46**, 1257 (1981).
[26] R. B. Wiringa, V. G. J. Stoks, and R. Schiavilla, Phys. Rev. C **51**, 38 (1995).
[27] W. Grüebler *et al.*, Nucl. Phys. A **398**, 445 (1983).
[28] G. Rauprich *et al.*, Few-Body Syst. **5**, 67 (1988).
[29] K. Sagara, H. Oguri, S. Shimizu, K. Maeda, H. Nakamura, T. Nakashima, and S. Morinobu, Phys. Rev. C **50**, 576 (1994).
[30] H. Shimizu *et al.*, Nucl. Phys. A **382**, 242 (1982).
[31] H. Sakai *et al.*, Phys. Rev. Lett. **84**, 5288 (2000).
[32] K. Hatanaka *et al.*, Phys. Rev. C **66**, 044002 (2002).
[33] Y. Maeda *et al.*, Phys. Rev. C **76**, 014004 (2007).
[34] F. Sperisen *et al.*, Nucl. Phys. A **422**, 81 (1984).
[35] H. Witała *et al.*, Few-Body Syst. **15**, 67 (1993).
[36] K. Sekiguchi *et al.*, Phys. Rev. C **65**, 034003 (2002).
[37] K. Sekiguchi *et al.*, Phys. Rev. C **89**, 064007 (2014).
[38] M. Sawada *et al.*, Phys. Rev. C **27**, 1932 (1983).
[39] K. Ermisch *et al.*, Phys. Rev. C **71**, 064004 (2005).
[40] E. Epelbaum *et al.*, Eur. Phys. J. A **56**, 92 (2020), and references therein.
[41] H. Witała, J. Golak, and R. Skibinski, Phys. Rev. C **105**, 054004 (2022).
[42] G. Rauprich *et al.*, Nucl. Phys. A **535**, 313 (1991).
[43] M. Allet *et al.*, Few-Body Syst. **20**, 27 (1996).
[44] M. Zadro *et al.*, Nuovo Cimento A **107**, 185 (1994).
[45] S. Kimura *et al.*, Few-Body Syst. **54**, 367 (2013).
[46] H. Patberg *et al.*, Phys. Rev. C **53**, 1497 (1996).
[47] Y. Eguchi *et al.*, EPJ Web Conf. **3**, 04007 (2010).
[48] H. Witała, J. Golak, R. Skibiński, V. Soloviov, and K. Topolnicki, Phys. Rev. C **101**, 054002 (2020).